

Pentaquark $\Theta^+(1540)$ production in $\gamma N \rightarrow K\bar{K}N$

Yongseok Oh* and K. Nakayama†

*Department of Physics and Astronomy,
University of Georgia, Athens, Georgia 30602, U.S.A.*

T.-S.H. Lee‡

Physics Division, Argonne National Laboratory, Argonne, Illinois 60439, U.S.A.

(Dated: December 2, 2024)

Abstract

We investigate how the exotic pentaquark $\Theta(1540)$ baryon production can be identified in the $\gamma N \rightarrow K\bar{K}N$ reactions, focusing on the influence of the background (non- Θ production) mechanisms. By imposing the SU(3) symmetry and using various quark model predictions, we are able to fix the coupling constants for evaluating the so-called Drell diagrams, the $K\bar{K}$ production through the intermediate vector meson and tensor meson photoproduction, and the mechanisms involving intermediate $\Lambda(1116)$, $\Lambda(1405)$, $\Lambda(1520)$, $\Sigma(1193)$, $\Sigma(1385)$, and $\Delta(1232)$ states. The vector meson photoproduction part is calculated from a phenomenological model which describes well the experimental data at low energies. The charged tensor meson production is calculated from a one-pion-exchange model which describes well the total cross section data of $\gamma p \rightarrow a_2^+(1320)n$. We point out that the neutral tensor meson production can not be due to π^0 -exchange as done by Dzierba *et al.* [Phys. Rev. D **69**, 051901 (2004)] because of C parity. The neutral tensor meson production is estimated by considering the vector meson exchange and found to be too weak to generate any peak at the position near $\Theta(1540)$. For $\Theta(1540)$ production, we assume that it is an isoscalar and hence can only be produced in $\gamma n \rightarrow K^+K^-n$ and $\gamma p \rightarrow K^0\bar{K}^0p$ reactions, not in $\gamma p \rightarrow K^+K^-p$ and $\gamma n \rightarrow K^0\bar{K}^0n$. The total cross section data of $\gamma p \rightarrow K^+K^-p$ is thus used to fix the form factors which regularize the background amplitudes so that the signal of $\Theta(1540)$ in $\gamma n \rightarrow K^+K^-n$ and $\gamma p \rightarrow K^0\bar{K}^0p$ cross sections can be predicted. We find that the predicted K^+K^- and K^+n invariant mass distributions of the $\gamma n \rightarrow K^+K^-n$ reaction can qualitatively reproduce the shapes of the JLab data. However, the predicted $\Theta(1540)$ peak can not be identified unambiguously with the data. High statistics experiments are needed to resolve the problem. We also find that an even-parity Θ is more likely to be detected, while it will be difficult to identify an odd-parity Θ , even if it exists, from the background continuum, if its coupling constants are small as in the present quark model predictions. The predictions are given to show that the photon beam asymmetry and beam-target double asymmetry can be useful in further verifying the existence of $\Theta(1540)$ and identifying its parity.

PACS numbers: 13.60.Le, 13.60.Rj, 14.80.-j

*Electronic address: yoh@physast.uga.edu

†Electronic address: nakayama@uga.edu

‡Electronic address: lee@phy.anl.gov

I. INTRODUCTION

The recent interests in pentaquark baryons was initiated by the discovery of $\Theta^+(1540)$ by the LEPs Collaboration at SPring-8 [1] and the subsequent experiments [2, 3, 4, 5, 6, 7, 8, 9, 10, 11]. Candidates for exotic pentaquark states $\Xi(1862)$ and $\Theta_c(3099)$ were also observed [12, 13]. However, the signals for those exotic states could not be found in several recent experiments [14, 15, 16, 17, 18, 19, 20]. The existence of pentaquark baryons is thus not conclusive at the present time, despite more reports have been given on possible candidates for various crypto-exotic baryons [21, 22, 23, 24].

To make progress, both experimental and theoretical efforts are needed. Experimentally, several high statistics experiments have been planned [25] and some data have been obtained and are under analyses. On the theoretical side, it is necessary to understand the reaction mechanisms of the considered reactions and to investigate how the pentaquark states production can be identified from the experimental observables. In particular, one must explore whether the resonance-like peaks near $W \sim 1540$ MeV can be resulted from the background (non- Θ production) mechanisms, as emphasized by Dzierba *et al.* [26]. In this paper, we report on the progress we have made in this direction concerning the $\gamma N \rightarrow K\bar{K}N$ reactions.

The $\gamma N \rightarrow K\bar{K}N$ reaction has been used to observe the production of $\Theta(1540)$ through its decay into KN [1, 3, 4, 7, 10, 19].¹ We will take the effective Lagrangian approach to assume that the amplitudes of this reaction can be computed from the tree-diagrams. In addition to the Θ production amplitude, we compute all possible background (non- Θ production) amplitudes whose parameters can be fixed by the SU(3) symmetry or taken from various quark model predictions. Undoubtedly, there are some tree-diagrams which are kinematically allowed, but can not be evaluated because of the lack of information about the relevant coupling constants. So our effort represents just a step toward developing a model for more realistic production amplitudes. But it should be sufficient for exploring the question concerning how the pentaquark $\Theta(1540)$ can be identified from the observables of $\gamma N \rightarrow K\bar{K}N$ reaction.

We classify the possible tree diagrams into four types: the so-called Drell diagrams (Fig. 1), vector meson and tensor meson production background (Fig. 2), hyperon background (Fig. 5), and the $\Theta(1540)$ production amplitude (Fig. 6). Our objective is to explore the interplay between these tree diagrams in determining the following reactions:

$$\begin{aligned} \gamma p &\rightarrow K^+ K^- p, & \gamma n &\rightarrow K^+ K^- n, \\ \gamma p &\rightarrow K^0 \bar{K}^0 p, & \gamma n &\rightarrow K^0 \bar{K}^0 n. \end{aligned} \quad (1)$$

The parameters as well as the form factors for evaluating these diagrams will be explained in detail in Section II.

There exist several investigations of the reactions listed in Eq. (1) in conjunction with the observation of $\Theta(1540)$. The background tree-diagrams considered by these works are summarized in Table I. In the very first investigation of $\gamma n \rightarrow K^+ K^- n$ by Nakayama and Tsushima (NT) [28], the Drell diagrams, vector meson background, and hyperon background are considered. But the tensor meson background was not included. Their hyperon background includes the $\Sigma(1193)$ and $\Sigma(1660)$ states, while the Λ baryon resonances do not come into play in the considered $\gamma n \rightarrow K^+ K^- n$ reaction because of the isospin selection rule.

¹ Old experiments to find the pentaquark states using this reaction can be found, e.g., in Ref. [27].

Models	Drell diagrams	Vector meson background	Tensor meson background	Hyperon background
NT [28]	✓	✓		✓
DKSTS [26]		✓	✓	
Roberts [30]	✓	✓		✓
TEHN [31]		✓	✓	
This work	✓	✓	✓	✓

TABLE I: Comparison of the models for $\gamma N \rightarrow K\bar{K}N$ as a background for the $\Theta(1540)$ production in the literature. See the text for the details.

The investigation of the $\gamma n \rightarrow K^+K^-n$ reaction by Dzierba *et al.* (DKSTS) [26] was motivated by an old experiment [29] on $\pi^-p \rightarrow K^-X$ reaction which was aimed at searching for the Θ baryon(s). With 8 GeV pion beams, this experiment found two peaks at $W = 1590$ and 1950 MeV in the KN channel. However, these peak positions moved to 1500 and 1800 MeV as the pion beam energy was lowered to 6 GeV. They hence concluded that the most natural explanation was to ascribe the peaks to the background production mechanisms, especially to the higher-spin meson production. Motivated by this analysis, Dzierba *et al.* claimed the possibility that the peak at 1540 MeV in $\gamma n \rightarrow K^+K^-n$ may come from the tensor meson photoproduction background. However, other production mechanisms such as Drell diagrams and hyperon backgrounds were not included in their investigation, as indicated in Table I. We will discuss this work in more detail later.

In Ref. [30], Roberts studied the contributions of Θ to the invariant mass distributions of $\gamma N \rightarrow K\bar{K}N$ reactions listed in Eq. (1). In addition to including many Λ and Σ baryons, he included vector meson production, but neglected the tensor meson production. He also explored how the $\gamma N \rightarrow K\bar{K}N$ observables can be used to distinguish the spin-parity of $\Theta(1540)$ by considering $J^P = \frac{1}{2}^\pm$ or $\frac{3}{2}^\pm$ for $\Theta(1540)$.

Titov *et al.* (TEHN) [31] investigated the effects of the scalar meson, vector meson, and tensor meson production background on the $\gamma N \rightarrow K\bar{K}N$ reactions. They found that the ϕ meson photoproduction due to the Pomeron-exchange is the major background mechanism. This result was obtained from using a phenomenological model which includes the meson exchanges and Pomeron exchange and can describe well the ϕ photoproduction data. The main emphasis in Ref. [31] was to explore the sensitivity and/or insensitivity of various spin asymmetries to the parity of Θ by improving on the work of Ref. [28]. However, the Drell diagrams and hyperon background were not included in this investigation.

As indicated in the last row of Table I, we consider in this work all four classes of the background amplitudes. Therefore, the present work represents an extension of the work initiated by Nakayama and Tsushima [28] toward developing a more realistic model of the $\gamma N \rightarrow K\bar{K}N$ reactions in order to extract relevant information concerning the pentaquark Θ . The main challenge here is to find the coupling constants which are needed to evaluate all possible tree diagrams. Undoubtedly, no progress can be made unless some truncations and approximations are taken. We impose the SU(3) symmetry and only keep the tree diagrams whose coupling constants can be either determined from using the information given by the Particle Data Group (PDG) or taken from various quark model predictions. Thus, we only consider the rather well-known hyperons, namely, $\Lambda(1116)$, $\Lambda(1405)$, $\Lambda(1520)$, $\Sigma(1193)$, and $\Sigma(1385)$ to evaluate the hyperon background (Fig. 5). The photo-transitions among those hyperons and the $\Delta \rightarrow N\gamma$ transition are also included. For the background amplitudes

with vector meson and tensor meson production (Fig. 2), the $\gamma N \rightarrow (V, T)N$ amplitudes are generated from the available phenomenological models which are constrained by the total cross section data of photoproduction of vector mesons (ρ , ω , ϕ) and tensor meson [$a_2^+(1320)$].

Another feature of our approach is regularizing each vertex in the considered tree diagrams by a form factor which depends on the mass and squared momentum of the exchanged particles. By following the methods of Refs. [32, 33, 34], the gauge invariance is recovered by introducing contact diagrams. We extend the methods of Refs. [32, 33, 34] for the two-body final state to the three-body final state with some modifications. The cutoff parameters of the form factors are determined by the available data of the $\gamma p \rightarrow K^+ K^- p$ reaction, which are then used to compute various observables. Thus our procedure in introducing the form factors is different from all the models listed in Table I, such as no form factor in the work of Ref. [28] and the use of the same form factor for all diagrams in the approach of Ref. [30].

We are also motivated by the question concerning the quantum numbers of $\Theta(1540)$. In Ref. [4], SAPHIR Collaboration claims non-existence of $\Theta(1540)$ in $K^+ p$ channel while they could confirm the peak of $\Theta(1540)$ in $K^+ n$ channel. This leads to the conclusion that the observed $\Theta(1540)$ is isosinglet and it belongs to baryon antidecuplet.² However, the spin-parity quantum numbers of Θ are still under debate. Theoretically, uncorrelated quark models [36], QCD sum rules [37], lattice QCD [38] favors odd-parity of $\Theta(1540)$, while even-parity is predicted by correlated quark models [39, 40, 41] and soliton models [42]. In addition, there is a debate on the parity of Θ in lattice calculation [43] and the parity-flip was claimed in QCD sum rules [44] with heavier anti-quark. (See also Refs. [45] for the status of QCD sum rules calculation.) However, most models identify the $\Theta(1540)$ as a member of the antidecuplet with spin-1/2. We therefore will use this assumption in this work. To be more specific, we follow the observations of Ref. [4] to assume that Θ is of isosinglet and hence can only be produced via the mechanisms of Fig. 6 in $\gamma n \rightarrow K^+ K^- n$ and $\gamma p \rightarrow K^0 \bar{K}^0 p$ of Eq. (1). The other two processes in Eq. (1) will also be considered for providing information to constrain the background (non- Θ production) amplitude by using the available data. We will also predict how the observables of $\gamma n \rightarrow K^+ K^- n$ depend on the parity of $\Theta(1540)$, as done in Refs. [46, 47, 48, 49, 50, 51, 52, 53, 54, 55] for the other reactions.

This paper is organized as follows. In Section II, we present our model for $K\bar{K}$ pair photoproduction reactions listed in Eq. (1). The form of the employed effective Lagrangians is given explicitly and the determination of their coupling constants is also discussed in detail. We present our results on the cross sections and spin asymmetries in Section III. A summary is given in Sect. IV and the details for tensor meson properties and form factors are given in Appendixes.

II. $K\bar{K}$ PAIR PHOTOPRODUCTION FROM THE NUCLEON

As mentioned in Section I, we will investigate all four reactions listed in Eq. (1) by considering the tree-diagrams illustrated in Fig. 1 for the Drell mechanisms, Fig. 2 for the production through vector meson and tensor meson photoproduction, Fig. 5 for the

² Flavor SU(3) symmetry allows three kinds of Θ baryons in quark models; isosinglet in antidecuplet, isovector in **27**-plet, and isotensor in **35**-plet [35].

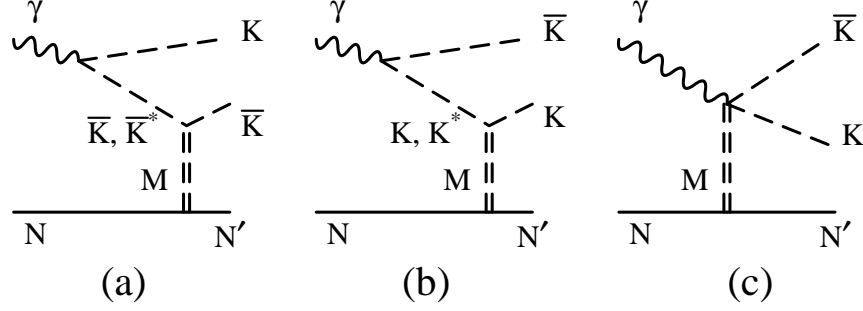


FIG. 1: Drell diagrams for $\gamma N \rightarrow K\bar{K}N$. Here M stands for a vector meson ($V = \rho, \omega$) or a pseudoscalar meson ($\varphi = \pi, \eta$).

hyperon background, and Fig. 6 for the Θ production. The effective Lagrangians needed for calculating each class of these tree diagrams will be given explicitly in the following subsections. The determinations of the relevant coupling constants will be discussed in detail.

A. Drell diagrams

For the Drell diagrams (Fig. 1), the incoming photon is converted into a $K\bar{K}$ pair or a $K\bar{K}^*$ ($\bar{K}K^*$) pair which then interact with the nucleon by meson exchanges. For the intermediate $K\bar{K}$ pair, we consider the vector meson exchanges. The effective Lagrangians for defining these amplitudes are

$$\begin{aligned}
\mathcal{L}_{\gamma KK} &= -ieA_\mu (K^- \partial^\mu K^+ - \partial^\mu K^- K^+), \\
\mathcal{L}_{VKK} &= -ig_{VKK} (\partial^\mu \bar{K} V_\mu K - \bar{K} V_\mu \partial^\mu K), \\
\mathcal{L}_{VNN} &= -g_{VNN} \bar{N} \left\{ \gamma^\mu V_\mu - \frac{\kappa_V}{2M_N} \sigma^{\mu\nu} \partial_\nu V_\mu \right\} N, \\
\mathcal{L}_{\gamma VKK} &= -eg_{VKK} \bar{K} [(1 + \tau_3)/2, V_\mu]_+ K A^\mu,
\end{aligned} \tag{2}$$

where $[A, B]_+ = AB + BA$, $V = (\rho, \omega, \phi)$, A_μ is the photon field, and the kaon isodoublets are defined as

$$K = \begin{pmatrix} K^+ \\ K^0 \end{pmatrix}, \quad \bar{K} = (K^-, \bar{K}^0). \tag{3}$$

We follow Ref. [56] to set³

$$\begin{aligned}
g_{\rho NN} &= 3.1, & \kappa_\rho &= 2.0, \\
g_{\omega NN} &= 10.3, & \kappa_\omega &= 0.0.
\end{aligned} \tag{4}$$

The exchange of ϕ meson is neglected by taking the simplest OZI rule prediction, $g_{\phi NN} = \kappa_\phi = 0$.

³ The Bonn potential gives $\kappa_\rho \approx 6.0$ [57], which is larger than the value in Eq. (4). We found that our results on the $\gamma N \rightarrow K\bar{K}N$ reaction are not sensitive to this coupling constant.

We next need to define the vertices connecting the kaons and vector mesons in Fig. 1. This is done by using the following SU(3) symmetric Lagrangian,

$$\begin{aligned}\mathcal{L}_{VPP} &= -\frac{ig_{VPP}}{\sqrt{2}} \text{Tr}\{V_\mu(P\partial^\mu P - \partial^\mu PP)\}, \\ \mathcal{L}_{VVP} &= g_{VVP}\varepsilon^{\mu\nu\alpha\beta} \text{Tr}(\partial_\mu V_\nu\partial_\alpha V_\beta P),\end{aligned}\quad (5)$$

where

$$P = \begin{pmatrix} \frac{1}{\sqrt{6}}\eta + \frac{1}{\sqrt{2}}\boldsymbol{\pi} \cdot \boldsymbol{\tau} & K \\ \frac{1}{\sqrt{2}}\eta & -\frac{2}{\sqrt{6}}\eta \end{pmatrix}, \quad V = \begin{pmatrix} \frac{1}{\sqrt{2}}\omega + \frac{1}{\sqrt{2}}\boldsymbol{\rho} \cdot \boldsymbol{\tau} & K^* \\ \frac{1}{\sqrt{2}}\omega & -\phi \end{pmatrix}.$$
 (6)

The K^* isodoublets are defined by the same way as in Eq. (3). The SU(3) symmetry relations lead to

$$g_{\rho KK} = g_{\omega KK} = g_{\rho\pi\pi}/2 = 3.02. \quad (7)$$

For the intermediate $K\bar{K}^*$ or $\bar{K}K^*$ pair in Fig. 1, we consider the pseudoscalar meson exchanges. The photon coupling is defined by

$$\begin{aligned}\mathcal{L}_{\gamma K^*K} &= g_{\gamma K^*K}^0 \varepsilon^{\mu\nu\alpha\beta} \partial_\mu A_\nu \left(\partial_\alpha K_\beta^{*0} \bar{K}^0 + \partial_\alpha K_\beta^{*0} K^{*0} \right) \\ &\quad + g_{\gamma K^*K}^c \varepsilon^{\mu\nu\alpha\beta} \partial_\mu A_\nu \left(\partial_\alpha K_\beta^{*-} K^+ + \partial_\alpha K_\beta^{*+} \bar{K}^- \right),\end{aligned}\quad (8)$$

with

$$g_{\gamma K^*K}^0 = -0.388 \text{ GeV}^{-1}, \quad g_{\gamma K^*K}^c = 0.254 \text{ GeV}^{-1}, \quad (9)$$

determined from the radiative decay widths of the neutral and charged K^* vector mesons. The couplings involving the pseudoscalar mesons π and η are defined by

$$\begin{aligned}\mathcal{L}_{K^*K\varphi} &= -ig_{K^*K\varphi} \left(\bar{K} \partial^\mu \varphi K_\mu^* - \bar{K}_\mu^* \partial^\mu \varphi K \right), \\ \mathcal{L}_{\varphi NN} &= \frac{g_{\varphi NN}}{2M_N} \bar{N} \gamma^\mu \gamma_5 \partial_\mu \varphi N,\end{aligned}\quad (10)$$

where $\varphi = \boldsymbol{\tau} \cdot \boldsymbol{\pi}, \eta$ and $N = (p, n)^T$. We choose the usual $g_{\pi NN}^2/(4\pi) = 14.3$ and use the SU(3) relation to set $g_{\eta NN}^2/(4\pi) = 1.0$. By using the experimental value for $\Gamma(K^* \rightarrow K\pi)$ and $\Gamma(K^* \rightarrow K\pi) = (g_{K^*K\pi}^2/8\pi M_{K^*}^2) p_\pi^3$, we find that

$$g_{K^*K\pi} = 6.56. \quad (11)$$

This value is close to the SU(3) value, $g_{K^*K\pi} = g_{\rho\pi\pi} = 6.04$. For $g_{K^*K\eta}$, we use the SU(3) relation,

$$g_{K^*K\eta} = \sqrt{3}g_{K^*K\pi} = 11.36 \quad (12)$$

In the diagrams of Fig. 1, the $K\bar{K}^*$ or $\bar{K}K^*$ intermediate states can also interact with the nucleon via vector meson exchanges. This can be calculated from the Lagrangian derived from \mathcal{L}_{VVP} of Eq. (5),

$$\mathcal{L}_{K^*KV} = g_{K^*KV} \varepsilon^{\mu\nu\alpha\beta} \bar{K} \partial_\mu V_\nu \partial_\alpha K_\beta^* + \text{H.c.}, \quad (13)$$

where

$$g_{K^*K\rho} = g_{K^*K\omega} = g_{\omega\rho\pi}/2, \quad g_{K^*K\phi} = g_{\omega\rho\pi}/\sqrt{2}. \quad (14)$$

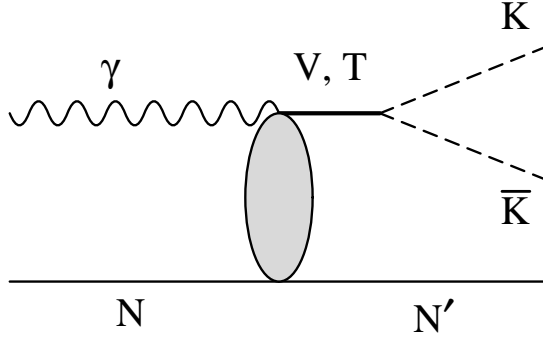


FIG. 2: Vector and tensor meson photoproduction contributions to $\gamma N \rightarrow K\bar{K}N$. Here V stands for a vector meson ($V = \rho, \omega, \phi$) and T for a tensor meson ($T = a_2, f_2$).

The above coupling constants can then be fixed by using the hidden gauge approach [58] to set

$$g_{\omega\rho\pi} = \frac{N_c g_\rho^2}{8\pi^2 f_\pi} = 14.9 \text{ GeV}^{-1}, \quad (15)$$

where $N_c = 3$, $g_\rho = g_{\rho\pi\pi}$, and $f_\pi = 93 \text{ MeV}$.

B. Vector meson background

As shown in Fig. 2, the vector meson background amplitude is determined by a vector meson photoproduction amplitude and the $V \rightarrow K\bar{K}$ vertex function defined by \mathcal{L}_{VKK} of Eq. (2). The resulting $\gamma N \rightarrow K\bar{K}N$ amplitude can be written as

$$\mathcal{M} = \bar{u}_{N'}(p') \mathcal{M}^\mu \varepsilon_\mu u_N(p), \quad (16)$$

where $u_N(p)$ is the Dirac spinor of a nucleon with momentum p , ε_μ is the photon polarization vector, p and p' are the momenta of the initial and final nucleon, respectively. The dynamics of Eq. (16) is contained in the following invariant amplitude,

$$\mathcal{M}^\mu = \mathcal{M}^{\nu\mu}(\gamma N \rightarrow VN) \frac{g_{VKK}}{(q_1 + q_2)^2 - M_V^2} (q_1 - q_2)_\nu F_V^{(i)}, \quad (17)$$

where q_1 and q_2 are the momenta of the outgoing K and \bar{K} , $F_V^{(i)}$ depends on the channel quantum number i as well as a form factor (28) which takes into account the off-shell-ness of the intermediate vector meson. The needed coupling constants g_{VKK} with $V = \rho, \omega$ have been given in Eq. (7). For ϕ decay, we here use $g_{\phi KK} = -4.49$ deduced from the experimental data of $\Gamma(\phi \rightarrow K^+ K^-)$ [59], while the phase is taken from the SU(3) symmetry. The photoproduction amplitude $\mathcal{M}^{\nu\mu}(\gamma N \rightarrow VN)$ is generated from a phenomenological model within which the blob in Fig. 2 includes Pomeron exchange, π , f_2 , and other meson exchanges, and the direct and crossed nucleon terms. The details of this model can be found in Refs. [60] and will not be repeated here. The finite decay width of vector mesons is included by replacing M_V by $M_V - i\Gamma_V/2$ in Eq. (17).

C. Tensor meson background

The tensor meson photoproduction contribution to $\gamma N \rightarrow K\bar{K}N$ is particularly interesting since it was suggested in Ref. [26] that this mechanism can generate a peak near 1540 MeV in the KN invariant mass distribution of the $\gamma n \rightarrow K^+K^-n$ reaction and hence the discovery of $\Theta(1540)$ pentaquark baryon is questionable. In this subsection, we explore this mechanism in more detail.

As illustrated in Fig. 2, the tensor meson photoproduction contribution is very similar to the vector meson photoproduction contribution. Its contribution to the $\gamma N \rightarrow K\bar{K}N$ amplitude is of the same structure of Eqs. (16)-(17) and can be written as

$$\mathcal{M} = \bar{u}_{N'}(p') \mathcal{M}^\mu \varepsilon_\mu u_N(p). \quad (18)$$

The main dynamics of Eq. (18) is contained in

$$\mathcal{M}^\mu = \mathcal{M}^{\gamma\delta,\mu}(\gamma N \rightarrow TN) \frac{2G_{TKK}}{M_T} \frac{P_{\gamma\delta;\rho\sigma}}{(q_1 + q_2)^2 - M_T^2} q_1^\rho q_2^\sigma F_T^{(i)}, \quad (19)$$

where q_1 and q_2 are the momenta of the outgoing K and \bar{K} . $F_T^{(i)}$ includes the constant depending on the channel i and the form factor. Here the $T \rightarrow K\bar{K}$ decay vertex is defined by the following tensor structure associated with a spin $J = 2$ particle, whose propagator contains

$$P^{\mu\nu;\rho\sigma} = \frac{1}{2} (\bar{g}^{\mu\rho} \bar{g}^{\nu\sigma} + \bar{g}^{\mu\sigma} \bar{g}^{\nu\rho}) - \frac{1}{3} \bar{g}^{\mu\nu} \bar{g}^{\rho\sigma}, \quad (20)$$

with

$$\bar{g}^{\mu\nu} = -g^{\mu\nu} + \frac{1}{M_T^2} p^\mu p^\nu, \quad (21)$$

where p^μ is the momentum of the tensor meson. The coupling constant G_{TKK} in Eq. (19) is defined by the Lagrangian

$$\mathcal{L}_{TKK} = -\frac{2G_{TKK}}{M_T} \partial_\mu \bar{K} T^{\mu\nu} \partial_\nu K, \quad (22)$$

where the kaon isodoublets are defined in Eq. (3) and $T^{\mu\nu} = f^{\mu\nu}$ or $\boldsymbol{\tau} \cdot \mathbf{a}^{\mu\nu}$, with $f^{\mu\nu}$ and $a^{\mu\nu}$ denoting the isoscalar $f_2(1275)$ and isovector $a_2(1320)$ tensor meson field, respectively. Some details about \mathcal{L}_{TKK} can be found in Appendix A. Using the experimental data [59], $\Gamma(f_2 \rightarrow K\bar{K})_{\text{expt.}} \approx 8.6$ MeV and $\Gamma(a_2 \rightarrow K\bar{K})_{\text{expt.}} \approx 5.24$ MeV, Eq. (22) leads to

$$G_{fKK} = 7.15, \quad G_{aKK} = 4.89. \quad (23)$$

In this work, we neglect the contribution from $f_2'(1525)$ meson since it can be produced favorably only at energies much higher than the region considered in this work. The finite decay width of tensor mesons is included by replacing M_T by $M_T - i\Gamma_T/2$ in its propagator.

We now turn to discussing the calculations of the tensor meson photoproduction amplitude $\mathcal{M}^{\alpha\beta,\mu}$ of Eq. (19). We note here that the tensor meson photoproduction mechanisms depend very much on the charge of the produced tensor mesons. In particular, the one-pion exchange is known [61, 62, 63] to be the dominant mechanism for charged tensor meson production, while it is not allowed in the neutral tensor meson production because of C parity. Thus the claim made by Dzierba *et al.* [26] concerning the peak at $W \sim 1540$ MeV generated by the neutral tensor production must be re-examined. This will be our focus by exploring the contributions from the vector meson exchange mechanisms.

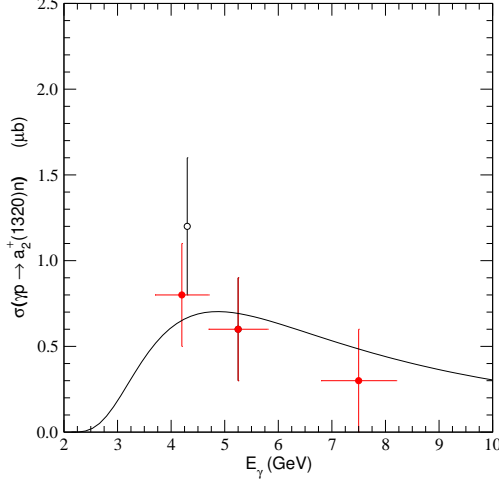


FIG. 3: Total cross section for charged tensor meson photoproduction, $\gamma p \rightarrow a_2^+(1320)n$. Experimental data are from Refs. [61] (\circ) and [62] (\bullet).

1. charged tensor meson photoproduction

We first calculate the charged tensor meson photoproduction, $\gamma p \rightarrow a_2^+(1320)n$ to explore the one-pion exchange model. This can be done by using the following interaction Lagrangian [64] which defines the $a_2\gamma\pi$ coupling,

$$\mathcal{L}_{a_2\gamma\pi} = \frac{g_{a_2\gamma\pi}}{M_a^2} \varepsilon^{\mu\nu\alpha\beta} \partial_\mu A_\nu a_{\alpha\lambda}^\pm (\partial^\lambda \partial_\beta \pi^\mp). \quad (24)$$

The decay width $\Gamma(a_2^\pm \rightarrow \pi^\pm \gamma)$ then reads

$$\Gamma(a_2^\pm \rightarrow \pi^\pm \gamma) = \frac{g_{a_2\gamma\pi}^2}{40\pi} \frac{p_\gamma^5}{M_a^4}, \quad (25)$$

where $p_\gamma = (M_a^2 - M_\pi^2)/2M_a$. Using $\Gamma(a_2 \rightarrow \gamma\pi)_{\text{expt.}} \approx 0.29$ MeV, we get

$$g_{a_2\gamma\pi} \approx 0.96. \quad (26)$$

Then the $\gamma p \rightarrow a_2^+(1320)n$ amplitude due to one-pion-exchange is obtained as

$$\mathcal{M}^{\mu\nu,\alpha} = \frac{\sqrt{2}g_{\pi NN}g_{a_2\gamma\pi}}{M_a^2} \frac{1}{(p-p')^2 - M_\pi^2} \varepsilon^{\rho\alpha\mu\sigma} k_\rho (q-k)^\nu (q-k)_\sigma \gamma_5 F(M_\pi, (k-q)^2), \quad (27)$$

where k is the photon momentum and q is the tensor meson momentum. The form factor is introduced in the form of

$$F(M, r) = \left(\frac{\Lambda^4}{\Lambda^4 + (r - M^2)^2} \right)^2. \quad (28)$$

We adjust the cutoff Λ of the form factor to fit the total cross section of $\gamma p \rightarrow a_2^+(1320)n$. With $\Lambda = 0.45$ GeV, the result is shown in Fig. 3. Therefore, we confirm that the photoproduction of charged a_2 meson can be reasonably described by the one-pion-exchange [61, 62, 63].

Decay	Decay width (keV)	$g_{TV\gamma}$
$f_2 \rightarrow \rho\gamma$	254	0.14
$f_2 \rightarrow \omega\gamma$	27	0.048
$f_2 \rightarrow \phi\gamma$	1.3	-0.022
$f_2' \rightarrow \rho\gamma$	4.8	0.0145
$f_2' \rightarrow \omega\gamma$	~ 0	~ 0
$f_2' \rightarrow \phi\gamma$	104	0.10
$a_2 \rightarrow \rho\gamma$	28	0.044
$a_2 \rightarrow \omega\gamma$	247	0.134
$a_2 \rightarrow \phi\gamma$	0.8	-0.015

TABLE II: Decay widths and couplings for $T \rightarrow V\gamma$ decay in a covariant quark model [68].

2. neutral tensor meson photoproduction

In Ref. [26], the authors used one-pion-exchange for neutral tensor meson photoproduction by extending the model for charged tensor meson photoproduction. However, the one-pion-exchange is *not allowed* for neutral tensor meson photoproduction because of the C -parity. Instead, we expect that the vector-meson exchange is the dominant process at low energies since the lightest mesons with $C = -1$ are the neutral vector mesons, ρ^0 and ω . At high energies, the Odderon exchange, a partner of the Pomeron with odd C parity, is suggested as the major production mechanism and in fact neutral tensor meson photoproduction process has been suggested to study the Odderon exchange [65]. Since the role of the Odderon exchange is not clearly known, especially at low energies, we will mainly consider the vector-meson exchange for the production mechanism of neutral tensor meson photoproduction in the energy region of our interest, i.e., $E_\gamma \leq 3$ GeV.

To calculate the vector meson exchange amplitude, we need to first define the $TV\gamma$ coupling, where $T = f_2, a_2$ and $V = \rho, \omega, \phi$. This can be determined by considering the tensor meson decay amplitude which can be written in the most general form as [66]

$$\langle \gamma(k)V(k')|T \rangle = \frac{1}{M_T} \epsilon^\kappa \epsilon'^\lambda \epsilon^{\mu\nu} A_{\kappa\lambda\mu\nu}(k, k'), \quad (29)$$

where

$$\begin{aligned} A_{\kappa\lambda\mu\nu}(k, k') = & \frac{f_{TV\gamma}}{M_T^3} [g_{\kappa\lambda}(k \cdot k') - k'_\kappa k_\lambda] (k - k')_\mu (k - k')_\nu \\ & + g_{TV\gamma} [g_{\kappa\lambda}(k - k')_\mu (k - k')_\nu + g_{\lambda\mu} k'_\kappa (k - k')_\nu + g_{\lambda\nu} k'_\kappa (k - k')_\mu \\ & - g_{\kappa\mu} k_\lambda (k - k')_\nu - g_{\kappa\nu} k_\lambda (k - k')_\mu - 2k \cdot k' (g_{\kappa\mu} g_{\lambda\nu} + g_{\kappa\nu} g_{\lambda\mu})]. \quad (30) \end{aligned}$$

The above form is known to give better descriptions of the known tensor meson radiative decays [67]. For simplicity, we will take the assumption of tensor meson dominance which leads to $f_{TV\gamma} \approx 0$ [66]. Without the $f_{TV\gamma}$ term, Eq. (30) is equivalent to that of Ref. [31] except for the factor of 2 difference in the definition of the coupling constant $g_{TV\gamma}$. In the present calculation, we take $g_{TV\gamma}$ from the covariant quark model predictions [68], which gives reasonable description of the known radiative decay widths of vector and tensor mesons. These values are listed in Table II along with the predicted decay widths. The details on the calculation of the radiative decays of tensor mesons are given in Appendix A.

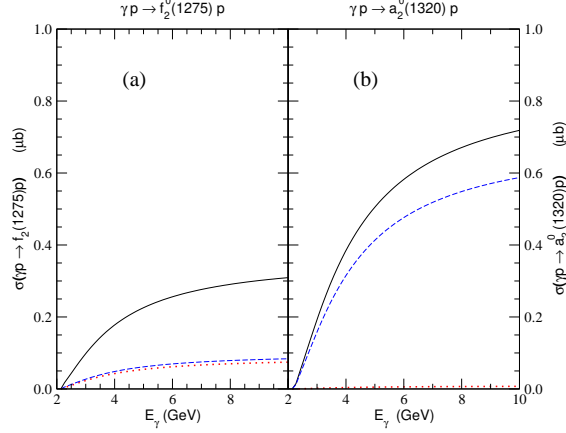


FIG. 4: Total cross section for neutral tensor meson photoproduction, (a) $\gamma p \rightarrow f_2^0(1275)p$ and (b) $\gamma p \rightarrow a_2^0(1320)p$. The dotted lines are from ρ meson exchange and the dashed lines from ω meson exchange. The solid lines are their sums.

With the $TV\gamma$ coupling fixed and the VNN coupling defined in the previous subsection, we can write the $\gamma p \rightarrow Tp$ amplitude as

$$\begin{aligned} \mathcal{M}^{\mu\nu,\alpha} = & -\frac{1}{M_T} A^{\alpha\beta\mu\nu}(k, q-k) \frac{C_{VNN} g_{VNN}}{(p-p')^2 - M_V^2} \left\{ g_{\beta\delta} - \frac{1}{M_V^2} (p-p')_\beta (p-p')_\delta \right\} \\ & \times \left\{ \gamma^\delta - i \frac{\kappa_V}{2M_N} \sigma^{\delta\lambda} (p-p')_\lambda \right\}, \end{aligned} \quad (31)$$

with $C_{VNN} = -1$ for ρnn , and $C_{VNN} = 1$ for ρpp , ωpp , and ωnn . The form of $A^{\alpha\beta\mu\nu}(k, q-k)$ is defined by Eq. (30). The form factor (28) is also used here to regularize each vertex. However, the experimental data for neutral tensor meson photoproduction is very limited and uncertain and cannot be used to fix the cutoff parameter Λ .⁴ To estimate their contribution, we take a relatively large cutoff $\Lambda = 0.9$ GeV to calculate the total cross sections for $f_2^0(1275)$ and $a_2^0(1320)$ photoproduction. The results are shown in Fig. 4. We see that they are smaller than the charged tensor meson production cross sections shown in Fig. 3 when $E_\gamma \leq 5$ GeV. If a smaller cutoff such as $\Lambda = 0.45$ GeV employed in Fig. 3 is used, the predicted cross sections will be even smaller. We will use $\Lambda = 0.9$ GeV in our calculation as an estimate of an upper bound of the neutral tensor meson photoproduction contribution. This will allow us to examine whether a peak near 1540 MeV in KN invariant mass can be generated by neutral tensor meson photoproduction process in the $\gamma n \rightarrow K^+ K^- n$ reaction, as claimed in Ref. [26].

From our results, we also found that in the case of a_2^0 photoproduction, the ω meson exchange is dominant, while both the ω and ρ exchanges are comparable in f_2^0 photoproduction. This is because $g_{a_2\rho\gamma}/g_{a_2\omega\gamma} \sim 1/3$ and $g_{f_2\rho\gamma}/g_{f_2\omega\gamma} \sim 3$ as seen in Table II, while $g_{\rho^0 NN}/g_{\omega NN} \sim 1/3$. Thus the ρ meson exchange amplitude in a_2^0 photoproduction is suppressed by an order of magnitude than the ω meson exchange, while the ρ and ω meson

⁴ In this work, we do not use the data for the backward scattering cross sections for f_2 meson photoproduction of Ref. [69], which was obtained by hand-drawn curves and after corrections for unobserved decay modes.

exchanges have similar magnitude in f_2 photoproduction.⁵

D. Hyperon background

The hyperon backgrounds for $\gamma N \rightarrow K \bar{K} N$ were considered in Refs. [28, 30]. The main difficulty in estimating the hyperon background arises from the uncertainties of the coupling parameters of the hyperon resonances ($Y = \Lambda, \Sigma$). We, therefore, consider only the well-known hyperon resonances, i.e., $\Lambda(1116)$, $\Lambda(1405)$, $\Lambda(1520)$, $\Sigma(1193)$, and $\Sigma(1385)$. We take the pseudoscalar coupling of kaons with the spin $J = 1/2$ hyperons. For coupling with the spin $J = 3/2$ hyperons, we follow the Rarita-Schwinger formulation of Refs. [70, 71, 72, 73, 74]. The resulting hyperon background tree-diagrams are shown in Fig. 5. We note that Fig. 5(d) includes the photo-transitions among the hyperons. Furthermore, Figs. 5(c) and (e) contain strangeness $S = 0$ state N'' . We will only consider the possibilities that N'' is either the nucleon (N) or the Delta [$\Delta(1232)$], since the experimental information about the transitions from other higher mass nucleon resonances to hyperons is not well-known. Since we are using the pseudoscalar coupling for spin-1/2 baryons, there is no $\gamma K Y N$ contact interaction and hence we have five diagrams, Figs. 5(a)-(e) for the intermediate $\Lambda(1116)$, $\Lambda(1405)$, and $\Sigma(1193)$ when K^* intermediate state is neglected. But for spin-3/2 $\Lambda(1520)$ and $\Sigma(1385)$, the $\gamma K Y N$ contact interaction is induced and we have seven diagrams, namely, Figs. 5(a)-(g) in the absence of K^* intermediate state. Figures 5(h)-(i) account for the effects due to K^* intermediate state.

The Lagrangians defining the photon coupling with K and K^* in Figs. 5(a), (b), (h), and (i) have been specified in Eqs. (2) and (8). In the following, we will discuss how the other couplings are defined by using SU(3) symmetry, experimental information, and some hadron model predictions.

1. Baryon octet

The baryon octet included in our calculation of Figs. 5(a)-(e) are the nucleon (N), $\Lambda(1116)$, and $\Sigma(1193)$. Their interactions with the photon are defined by

$$\begin{aligned}
 \mathcal{L}_{\gamma NN} &= -e\bar{N} \left[A_\mu \gamma^\mu \frac{1 + \tau_3}{2} - \frac{1}{2M_N} (\kappa_s^N + \kappa_v^N \tau_3) \sigma_{\mu\nu} \partial^\nu A^\mu \right] N, \\
 \mathcal{L}_{\gamma\Lambda\Lambda} &= \frac{e\kappa^\Lambda}{2M_N} \bar{\Lambda} \sigma_{\mu\nu} \partial^\nu A^\mu \Lambda, \\
 \mathcal{L}_{\gamma\Sigma\Sigma} &= -e\bar{\Sigma} \left[A_\mu \gamma^\mu T_3 - \frac{1}{2M_N} (\kappa_s^\Sigma + \kappa_v^\Sigma T_3) \sigma_{\mu\nu} \partial^\nu A^\mu \right] \Sigma,
 \end{aligned} \tag{32}$$

⁵ Therefore, the present results are different from those of Ref. [31], where only the ω exchange for a_2^0 photoproduction and only the ρ exchange for f_2 photoproduction were considered. We also calculated neutral tensor meson photoproduction in Regge model by Reggeizing the vector meson exchange amplitudes. The obtained results show that the total cross section decreases with energy as expected, but we found that the maximum values obtained in Regge model without form factor are close to the ones given in Fig. 4 with the similar photon energy.

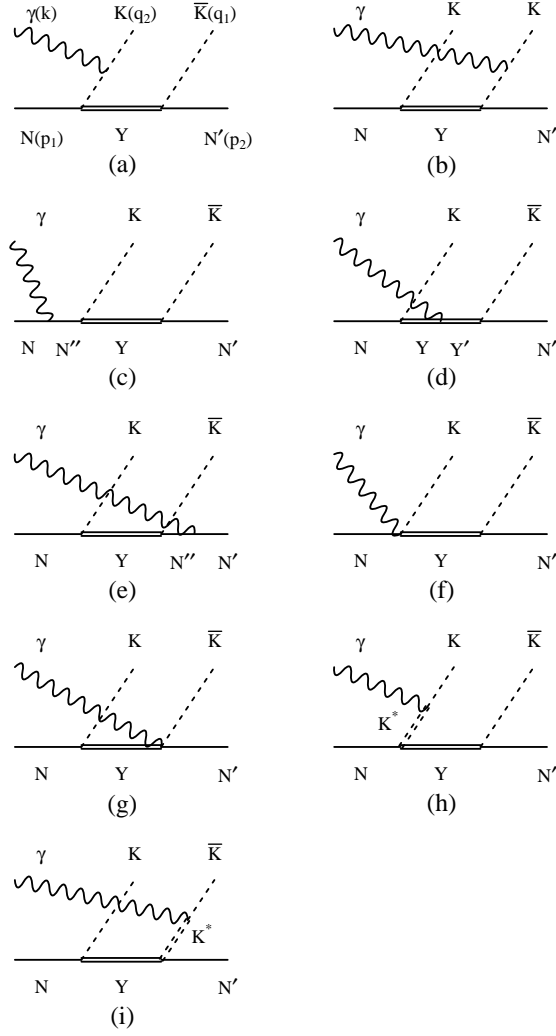


FIG. 5: $S = -1$ hyperon backgrounds to $\gamma N \rightarrow K\bar{K}N$.

where $T^3 = \text{diag}(1, 0, -1)$ and

$$\begin{aligned} \kappa_s^N &= \frac{1}{2}(\kappa_p + \kappa_n) = -0.06, & \kappa_v^N &= \frac{1}{2}(\kappa_p - \kappa_n) = 1.85, \\ \kappa^\Lambda &= -0.61, & \kappa_s^\Sigma &= \frac{1}{2}(\kappa_{\Sigma^+} + \kappa_{\Sigma^-}) = 0.65, & \kappa_v^\Sigma &= \frac{1}{2}(\kappa_{\Sigma^+} - \kappa_{\Sigma^-}) = 0.81. \end{aligned} \quad (33)$$

The numbers above are obtained by using the measured magnetic moments of the baryon octet [59], $\mu(p) = 2.79$, $\mu(n) = -1.91$, $\mu(\Lambda) = -0.61$, $\mu(\Sigma^+) = 2.46$, and $\mu(\Sigma^-) = -1.16$ in the nucleon magneton unit. To calculate the photo-transition of Σ into Λ in Fig. 5(d), we use

$$\mathcal{L}_{\gamma\Sigma\Lambda} = \frac{e\mu_{\Sigma\Lambda}}{2M_N} \bar{\Sigma}^0 \sigma_{\mu\nu} \partial^\nu A^\mu \Lambda + \text{H.c.}, \quad (34)$$

where $\mu_{\Sigma\Lambda} = -1.61 \pm 0.08$ as given by the Particle Data Group [59].

For meson-baryon interactions, we use the pseudoscalar coupling to write

$$\mathcal{L}_{K\Lambda N} = -ig_{\Lambda NK} \bar{N} \gamma_5 \Lambda K + \text{H.c.},$$

$$\mathcal{L}_{KN\Sigma} = -ig_{\Sigma NK}\bar{N}\gamma_5\boldsymbol{\tau}\cdot\Sigma K + \text{H.c.} \quad (35)$$

The flavor SU(3) symmetry relations evaluated with $d + f = 1$ give

$$g_{KN\Lambda} = -\frac{1}{\sqrt{3}}(1 + 2f)g_{\pi NN}, \quad g_{KN\Sigma} = (1 - 2f)g_{\pi NN}. \quad (36)$$

By using the empirical value $f/d = 0.575$, which gives $f = 0.365$ and $d = 0.635$, and $g_{\pi NN}^2/4\pi = 14$, we get

$$g_{KN\Lambda} = -13.24, \quad g_{KN\Sigma} = 3.58. \quad (37)$$

To calculate Figs. 5(h) and (i) with intermediate K^* , we use the following Lagrangian,

$$\mathcal{L}_{K^*NY} = -g_{K^*NY}\bar{N}\left(\gamma_\mu Y K^{*\mu} + \frac{\kappa_{K^*NY}}{2M_N}\sigma_{\mu\nu}Y\partial^\nu K^{*\mu}\right). \quad (38)$$

We use the values from the new Nijmegen potential [75] to define the coupling constants in the above equation,

$$\begin{aligned} g_{K^*N\Lambda} &= -6.11 \sim -4.26, & \kappa_{K^*N\Lambda} &= 0.436 \sim 0.474, \\ g_{K^*N\Sigma} &= -3.52 \sim -2.46, & \kappa_{K^*N\Sigma} &= -1.0 \sim -0.412. \end{aligned} \quad (39)$$

For our numerical calculation, the values in the right boundary are used.

2. Baryon decuplet

We now consider the couplings involving the members of the baryon decuplet, $\Delta(1232)$ and $\Sigma^*(1385)$, which are intermediate states in Figs. 5(a)-(g). The Lagrangians describing the photo-interaction of $\Sigma^*(1385)$ read

$$\begin{aligned} \mathcal{L}_{\gamma\Sigma^*\Sigma^*} &= e\bar{\Sigma}_\mu^* A_\alpha \Gamma_{\gamma\Sigma^*}^{\alpha,\mu\nu} \Sigma_\nu^*, \\ \mathcal{L}_{\gamma KN\Sigma^*} &= -i\frac{ef_{KN\Sigma^*}}{M_K} A^\mu \left(\bar{\Sigma}_\mu^{*0} p K^- + \sqrt{2}\bar{\Sigma}_\mu^{*-} n K^- - K^+ \bar{p} \Sigma_\mu^{*0} - \sqrt{2}K^+ \bar{n} \Sigma_\mu^{*-} \right), \end{aligned} \quad (40)$$

where [71]⁶

$$A_\alpha \Gamma^{\alpha,\mu\nu} = \left\{ g^{\mu\nu} \gamma^\alpha - \frac{1}{6}(\gamma^\mu \gamma^\nu \gamma^\alpha + \gamma^\alpha \gamma^\mu \gamma^\nu) \right\} A_\alpha T_3 - \frac{1}{2M_N} (\kappa_s^{\Sigma^*} + \kappa_v^{\Sigma^*} T_3) \sigma^{\alpha\beta} \partial_\beta A_\alpha g^{\mu\nu}, \quad (41)$$

and the coupling $f_{KN\Sigma^*}$ will be explained later. Since there is no experimental information for the magnetic moments of $\Sigma(1385)$, we make use of the following quark model predictions [77]

$$\mu(\Sigma^{*+}) = 3.15, \quad \mu(\Sigma^{*0}) = 0.36, \quad \mu(\Sigma^{*-}) = -2.43, \quad (42)$$

to obtain

$$\kappa_s^{\Sigma^*} = 0.36, \quad \kappa_v^{\Sigma^*} = 1.79. \quad (43)$$

⁶ There is an ambiguity with defining the non-minimal anomalous magnetic moment term. Here we follow Ref. [71]. Other definitions are discussed in Refs. [70, 76].

We next need to construct the photo-transition Lagrangians $\mathcal{L}_{\gamma N\Delta}$, $\mathcal{L}_{\gamma\Lambda\Sigma^*}$, and $\mathcal{L}_{\gamma\Sigma\Sigma^*}$. These can be fixed by considering the radiative decays of the decuplet baryons. The most well-studied is the $\Delta \rightarrow N\gamma$ transition which enters into Figs. 5(c) and (e). Here we follow Ref. [72] to write

$$\begin{aligned}\mathcal{L}_{\gamma N\Delta}^1 &= \frac{ieg_{1N\Delta}}{2M_N}\bar{\Delta}^\mu O_{\mu\lambda}(Z)\gamma_\nu\gamma_5 I^3\left(\frac{3}{2}, \frac{1}{2}\right)NF^{\nu\lambda} + \text{H.c.}, \\ \mathcal{L}_{\gamma N\Delta}^2 &= -\frac{eg_{2N\Delta}}{4M_N^2}\bar{\Delta}^\mu O_{\mu\nu}(Z)\gamma_5 I^3\left(\frac{3}{2}, \frac{1}{2}\right)(\partial_\lambda N)F^{\nu\lambda} + \text{H.c.},\end{aligned}\quad (44)$$

where $F^{\mu\nu}$ is the field strength tensor of the photon, $F^{\mu\nu} = \partial^\mu A^\nu - \partial^\nu A^\mu$, and we choose the off-shell parameters so that $O_{\mu\nu}(Z) = g_{\mu\nu}$. The isospin factor is calculated as

$$\bar{\Delta}I^3\left(\frac{3}{2}, \frac{1}{2}\right)N = \sqrt{\frac{2}{3}}\left(\bar{\Delta}^+p + \bar{\Delta}^0n\right). \quad (45)$$

The above Lagrangians lead to the following expression for calculating the radiative decay width of the Δ ,

$$\begin{aligned}\Gamma(\Delta \rightarrow N\gamma) &= \frac{p_\gamma^3}{72\pi M_\Delta^2}\left(\frac{e}{2M_N}\right)^2\left\{\left[g_{1N\Delta}(3M_\Delta + M_N) - g_{2N\Delta}\frac{M_\Delta}{2M_N}(M_\Delta - M_N)\right]^2\right. \\ &\quad \left.+ 3\left[g_{1N\Delta} - g_{2N\Delta}\frac{M_\Delta}{2M_N}\right]^2(M_\Delta - M_N)^2\right\}.\end{aligned}\quad (46)$$

It is well-known that the $g_{2N\Delta}$ term is sensitive to the $E2/M1$ ratio of $\Delta \rightarrow N\gamma$ decay. In this calculation, however, we assume that $g_{2N\Delta} = 0$, which gives somewhat large value, $\approx -6\%$, of $E2/M1$. However, our results show that the contributions from the ΔN transition to $\gamma N \rightarrow K\bar{K}N$ reaction are suppressed compared with the other contributions. Therefore the precise value of $g_{2N\Delta}$ is irrelevant to this calculation. Using $\Gamma(\Delta \rightarrow N\gamma)_{\text{expt.}} \approx 672$ keV, we then get

$$g_{N\Delta} = g_{1N\Delta} \approx 4.9, \quad (47)$$

which is close to the fitted value, ≈ 5.0 , of Ref. [72].

To calculate $Y \rightarrow Y'\gamma$ transition in Fig. 5(d), we consider the following Lagrangian,

$$\mathcal{L}_{\gamma BD} = \frac{ieg_{BD}}{2M_N}\bar{D}^\mu O_{\mu\lambda}(Z)\gamma_\nu\gamma_5 BF^{\nu\lambda} + \text{H.c.}, \quad (48)$$

where D^μ is the $\Sigma^*(1385)$ and B denotes for $\Lambda(1116)$ or $\Sigma(1193)$. There is no experimental information on the radiative decay widths for decuplet $\Sigma^*(1385)$ except some upper bounds. We therefore make use of the following quark model predictions [78],

$$\begin{aligned}\Gamma(\Sigma^{*0} \rightarrow \Lambda\gamma) &= 232 \text{ keV}, & \Gamma(\Sigma^{*+} \rightarrow \Sigma^+\gamma) &= 104 \text{ keV}, \\ \Gamma(\Sigma^{*0} \rightarrow \Sigma^0\gamma) &= 19 \text{ keV}, & \Gamma(\Sigma^{*-} \rightarrow \Sigma^-\gamma) &= 2.5 \text{ keV}.\end{aligned}\quad (49)$$

The above values then fix the coupling constants of $\mathcal{L}_{\gamma BD}$ as

$$g_{\Sigma^{*0}\Lambda} \approx 3.01, \quad g_{\Sigma^{*+}\Sigma^+} \approx 3.38, \quad g_{\Sigma^{*0}\Sigma^0} \approx 1.44, \quad g_{\Sigma^{*-}\Sigma^-} \approx 0.52. \quad (50)$$

We now will use the SU(3) symmetry to fix the couplings involving K mesons, baryon decuplet [$\Sigma^*(1385)$, $\Delta(1232)$] and baryon octet [N , $\Lambda(1116)$, $\Sigma(1193)$]. We start with the well-studied Lagrangian for the $\pi N\Delta$ interaction. We follow Refs. [73, 74] to write

$$\mathcal{L}_{\pi N\Delta} = \frac{f_{\pi N\Delta}}{m_\pi} \bar{\Delta}^\mu O_{\mu\nu}(Z) \mathbf{I}(\frac{3}{2}, \frac{1}{2}) \cdot \partial_\nu \boldsymbol{\pi} N + \text{H.c.}, \quad (51)$$

where the isospin transition matrix reads

$$\mathbf{I}(\frac{3}{2}, \frac{1}{2}) \cdot \boldsymbol{\pi} = -I_{3/2,1/2}^{(+1)} \pi^+ + I_{3/2,1/2}^{(-1)} \pi^- + I_{3/2,1/2}^{(0)} \pi^0, \quad (52)$$

with

$$I_{\frac{3}{2}, \frac{1}{2}}^{(+1)} = \frac{1}{\sqrt{6}} \begin{pmatrix} \sqrt{6} & 0 \\ 0 & \sqrt{2} \\ 0 & 0 \\ 0 & 0 \end{pmatrix}, \quad I_{\frac{3}{2}, \frac{1}{2}}^{(0)} = \frac{1}{\sqrt{6}} \begin{pmatrix} 0 & 0 \\ 2 & 0 \\ 0 & 2 \\ 0 & 0 \end{pmatrix}, \quad I_{\frac{3}{2}, \frac{1}{2}}^{(-1)} = \frac{1}{\sqrt{6}} \begin{pmatrix} 0 & 0 \\ 0 & 0 \\ \sqrt{2} & 0 \\ 0 & \sqrt{6} \end{pmatrix}. \quad (53)$$

With $O_{\mu\nu}(Z) = g_{\mu\nu}$ [73, 74] (see also Ref. [70]), the $\Delta \rightarrow \pi N$ decay width can be written as

$$\Gamma(\Delta \rightarrow N\pi) = \frac{p_\pi^3}{24\pi} \left(\frac{f_{\pi N\Delta}}{M_\pi} \right)^2 \frac{1}{M_\Delta^2} [(M_\Delta + M_N)^2 - M_\pi^2]. \quad (54)$$

Using $M_\Delta = 1232$ MeV and $\Gamma(\Delta \rightarrow N\pi) = 120$ MeV, we get⁷

$$f_{\pi N\Delta} = 2.23. \quad (55)$$

With the $\pi N\Delta$ coupling fixed, we then use the SU(3) relations,

$$\frac{f_{K\Sigma\Delta}}{M_K} = -\frac{f_{\pi N\Delta}}{M_N}, \quad f_{KN\Sigma^*} = \frac{1}{\sqrt{6}} f_{K\Sigma\Delta}, \quad (56)$$

to obtain

$$\begin{aligned} \mathcal{L}_{K\Sigma\Delta} &= \frac{f_{K\Sigma\Delta}}{M_K} \bar{\Delta}^\mu \mathbf{I}(\frac{3}{2}, \frac{1}{2}) \cdot \boldsymbol{\Sigma} \partial_\mu K + \text{H.c.}, \\ \mathcal{L}_{KN\Sigma^*} &= \frac{f_{KN\Sigma^*}}{M_K} \partial_\mu \bar{K} \bar{\boldsymbol{\Sigma}}^{*\mu} \cdot \boldsymbol{\tau} N + \text{H.c.} \end{aligned} \quad (57)$$

where

$$f_{K\Sigma\Delta} \approx -7.88, \quad f_{KN\Sigma^*} \approx -3.22. \quad (58)$$

In the numerical calculation, we use $f_{KN\Sigma^*} = -2.6$, which is within the range of SU(3) symmetry breaking.

The diagrams of Figs. 5(c) and (e) can have K interactions with the baryon decuplet $\Sigma(1385)$ and Δ . To determine these couplings using SU(3) relations, we again start with the $\pi\Delta\Delta$ interaction, which reads

$$\mathcal{L}_{\pi\Delta\Delta} = \frac{f_{\pi\Delta\Delta}}{M_\pi} \bar{\Delta}^\alpha O_{\alpha\beta}(Z) \gamma_\mu \gamma_5 \mathbf{I}(\frac{3}{2}, \frac{3}{2}) \cdot \partial^\mu \boldsymbol{\pi} O^{\beta\delta}(Z) \Delta_\delta. \quad (59)$$

⁷ If we use the pole mass $M_\Delta = 1211$ MeV, we get $f'_{\pi N\Delta} = 2.56$. In Ref. [56], $f_{\pi N\Delta}$ is estimated to be 2.05–2.12.

By using the quark model prediction [79] $f_{\pi\Delta\Delta}/f_{\pi NN} = 4/5$ ($f_{\pi NN} = g_{\pi NN} \frac{M_\pi}{2M_N}$), we find $f_{\pi\Delta\Delta} \approx 0.8$. The SU(3) relation

$$f_{K\Delta\Sigma^*} = -\sqrt{\frac{3}{2}} f_{\pi\Delta\Delta} \frac{M_K}{M_\pi} \approx 3.46, \quad (60)$$

then fixes the following Lagrangian for $K\Delta\Sigma^*$ interaction

$$\mathcal{L}_{K\Delta\Sigma^*} = \frac{f_{K\Delta\Sigma^*}}{M_K} \bar{\Delta}^\alpha O_{\alpha\beta}(Z) \gamma_\mu \gamma_5 O^{\beta\delta}(Z) \mathbf{I}(\frac{3}{2}, \frac{1}{2}) \cdot \Sigma_\delta^* \partial^\mu K. \quad (61)$$

Finally, we consider the interactions of baryon decuplet [$\Sigma^*(1358)$] with the vector mesons (K^*) in Figs. 5(h) and (i). In order to use the SU(3) symmetry relation, we start with the $\rho N\Delta$ interaction,

$$\mathcal{L}_{\rho N\Delta} = i \frac{f_{\rho N\Delta}}{M_\rho} \bar{\Delta}^\sigma O_{\sigma\mu}(Z) \gamma_5 \gamma_\nu \mathbf{T}(\frac{3}{2}, \frac{1}{2}) \cdot (\partial^\mu \boldsymbol{\rho}^\nu - \partial^\nu \boldsymbol{\rho}^\mu) N, \quad (62)$$

where the coupling constant can be fixed by the quark model relation [57],

$$f_{\rho N\Delta} = \frac{f_{\pi N\Delta} g_{\rho NN}}{f_{\pi NN}} \frac{M_\rho}{2M_N} (1 + \kappa_\rho). \quad (63)$$

By using $g_{\rho NN} = 3.1$ and $\kappa_\rho = 1.0$, we find $f_{\rho N\Delta} \approx 5.5$. This should be compared with the range 3.5–7.8 of Ref. [80]. By using the SU(3) relation

$$f_{K^* N \Sigma^*} = -\frac{f_{\rho N\Delta}}{\sqrt{6}} \frac{M_{K^*}}{M_\rho} \approx 2.59, \quad (64)$$

we then fix the $K^* N \Sigma^*$ coupling,

$$\mathcal{L}_{K^* N \Sigma^*} = i \frac{f_{K^* N \Sigma^*}}{M_{K^*}} (\partial^\mu K^{*\nu} - \partial^\nu K^{*\mu}) \bar{\Sigma}^{*\sigma} \cdot \boldsymbol{\tau} O_{\sigma\mu} \gamma_5 \gamma_\nu N. \quad (65)$$

With the above Lagrangians, we can evaluate all diagrams in Fig. 5 by specifying the propagator of spin-3/2 $\Sigma^*(1385)$ and $\Delta(1232)$. Here we follow Refs. [70, 71] and use the following Rarita-Schwinger form for the propagator of a spin-3/2 particle of a mass M_{Y^*} and momentum p ,

$$\tilde{\Delta}_{\mu\nu}(Y^*, p) = \frac{-i}{p^2 - M_{Y^*}^2} \Delta_{\mu\nu}(Y^*, p), \quad (66)$$

where

$$\Delta_{\mu\nu}(Y^*, p) = (\not{p} + M_{Y^*}) S_{\mu\nu}(Y^*, p) - \frac{2(p^2 - M_{Y^*}^2)}{3M_{Y^*}^2} [\gamma_\mu p_\nu + \gamma_\nu p_\mu - \gamma_\mu (\not{p} - M_{Y^*}) \gamma_\nu], \quad (67)$$

with

$$S^{\mu\nu}(Y^*, p) = -g^{\mu\nu} + \frac{1}{3} \gamma^\mu \gamma^\nu + \frac{1}{3M_{Y^*}} (\gamma^\mu p^\nu - \gamma^\nu p^\mu) + \frac{2}{3M_{Y^*}^2} p^\mu p^\nu. \quad (68)$$

The decay width of the decuplet is included by replacing M_{Y^*} by $M_{Y^*} - i\Gamma_{Y^*}/2$ in the propagator. Similar form of the propagator is also used for $N'' = \Delta$ in evaluating Fig. 5(c) and (e).

3. $\Lambda(1405)$

The $\Lambda(1405)$ with $J^P = \frac{1}{2}^-$ is also included in our calculation of Fig. 5(a)-(e). Its decay width is $\Gamma = 50 \pm 2$ MeV and it mostly decays into the $\Sigma\pi$ channel. To get its coupling with K , we consider scalar coupling SU(3) Lagrangian,

$$\mathcal{L}_{\Lambda_1} = -ig_{\Lambda_1} \bar{\Lambda}_1 (\bar{K}N + \bar{K}_c \Xi + \Sigma \cdot \boldsymbol{\pi} + \Lambda\eta) + \text{H.c.}, \quad (69)$$

where Λ_1 is the $\Lambda(1405)$ field. This leads to

$$\Gamma(\Lambda(1405) \rightarrow \Sigma\pi) = \frac{3g_{\Lambda_1}^2}{4\pi} \frac{p_\pi}{M_{\Lambda_1}} \left(\sqrt{M_\Sigma^2 + p_\pi^2} + M_\Sigma \right), \quad (70)$$

where M_{Λ_1} is the mass of $\Lambda(1405)$ and $p_\pi = \sqrt{\lambda(M_{\Lambda_1}^2, M_\Sigma^2, M_\pi^2)}/(2M_{\Lambda_1})$ with

$$\lambda(x, y, z) = x^2 + y^2 + z^2 - 2(xy + yz + zx). \quad (71)$$

So using $\Gamma(\Lambda(1405) \rightarrow \Sigma\pi)_{\text{expt.}} \approx 50$ MeV, we obtain $g_{\Lambda_1} \approx 0.13$ and the needed $KN\Lambda(1405)$ coupling can be computed from Eq. (69).

Figure 5(d) can have $\gamma\Lambda(1405)\Lambda(1405)$ vertex. This is calculated from

$$\mathcal{L}_{\gamma\Lambda_1\Lambda_1} = \frac{e\kappa_{\Lambda_1}}{2M_N} \bar{\Lambda}_1 \sigma_{\mu\nu} \partial^\nu A^\mu \Lambda_1, \quad (72)$$

where κ_{Λ_1} is the magnetic moment of $\Lambda(1405)$. There is no experimental information for the magnetic moment of $\Lambda(1405)$. So we have to rely on model predictions. It has been estimated to be $0.22 \sim 0.25$ in Skyrme model [81] and $0.24 \sim 0.45$ in a unitarized chiral perturbation theory [82]. Here we use $\kappa_{\Lambda_1} = 0.25$ in the nucleon magneton unit.

For the intermediate hyperon state in Fig. 5(d), we also include $\Lambda(1405) \rightarrow \Lambda(1116)\gamma$ and $\Lambda(1405) \rightarrow \Sigma(1193)\gamma$ couplings. They are defined by

$$\mathcal{L}_{\gamma Y \Lambda_1} = \frac{eg_{\gamma Y \Lambda_1}}{4(M_{\Lambda_1} + M_Y)} \bar{\Lambda}_1 \gamma_5 \sigma_{\mu\nu} Y F^{\nu\mu} + \text{H.c.}, \quad (73)$$

which leads to

$$\Gamma(\Lambda_1 \rightarrow Y\gamma) = \frac{\alpha_{\text{em}} g_{\gamma Y \Lambda_1}^2 p_\gamma^3}{(M_{\Lambda_1} + M_Y)^2}, \quad (74)$$

where $p_\gamma = (M_{\Lambda_1}^2 - M_Y^2)/(2M_{\Lambda_1})$. By using the quark model predictions [78]

$$\Gamma(\Lambda(1405) \rightarrow \Lambda\gamma) = 143 \text{ keV}, \quad \Gamma(\Lambda(1405) \rightarrow \Sigma^0\gamma) = 91 \text{ keV}, \quad (75)$$

the parameters for $\mathcal{L}_{\gamma Y \Lambda_1}$ are then fixed as

$$g_{\gamma\Lambda\Lambda_1} \approx 2.67, \quad g_{\gamma\Sigma\Lambda_1} \approx 3.34. \quad (76)$$

The predicted decay width $\Gamma(\Lambda(1405) \rightarrow \Sigma^{*0}(1385)\gamma) = 0.3$ keV is suppressed and not considered in this calculation.

4. $\Lambda(1520)$

We now consider the calculations of Fig. 5 with $Y = \Lambda(1520)$ which is a $J^P = \frac{3}{2}^-$ state. There is no information for the magnetic moment of $\Lambda(1520)$. We therefore neglect the tensor coupling of the electromagnetic interaction of $\Lambda(1520)$ by setting $\mu[\Lambda(1520)] = 0$. The coupling of $\Lambda(1520)$ with photon thus has the same form as the $\mathcal{L}_{\gamma\Sigma^*\Sigma^*}$ in Eq. (40) except that $\Lambda(1520)$ is a neutral particle.

For the $KN\Lambda(1520)$ (denoted as Λ') coupling, we write

$$\mathcal{L}_{KN\Lambda'} = \frac{f_{KN\Lambda'}}{M_K} \bar{\Lambda}'^\mu \gamma_5 \partial_\mu \bar{K} N + \text{H.c.}, \quad (77)$$

where Λ'^μ is the $\Lambda(1520)$ field. This gives the decay width of $\Lambda(1520) \rightarrow N\bar{K}$ as

$$\Gamma[\Lambda(1520) \rightarrow N\bar{K}] = \frac{1}{6\pi} \left(\frac{f_{KN\Lambda'}}{M_K} \right)^2 \frac{p_K^3}{M_{\Lambda'}} \left(\sqrt{M_N^2 + p_K^2} - M_N \right). \quad (78)$$

Using $\Gamma[\Lambda(1520) \rightarrow N\bar{K}]_{\text{expt.}} \approx 7 \text{ MeV}$, we have

$$f_{KN\Lambda'} \approx 10.92. \quad (79)$$

Figure 5(d) also includes the photon transition between $\Lambda(1520)$ and other hyperons. This is calculated by using the following Lagrangian [74],

$$\mathcal{L}_{\gamma Y\Lambda'} = \frac{ieg_1}{2M_Y} \bar{\Lambda}'^\mu O_{\mu\lambda\gamma\nu} Y F^{\nu\lambda} - \frac{eg_2}{4M_Y^2} \bar{\Lambda}'^\mu O_{\mu\nu} (\partial_\lambda Y) F^{\nu\lambda}. \quad (80)$$

Then we have

$$\begin{aligned} \Gamma(\Lambda' \rightarrow Y\gamma) = & \frac{\alpha_{\text{em}} p_\gamma^3}{48M_R^2 M_Y^2} \left[\left\{ g_1(3M_R + M_Y) - g_2 \frac{M_R}{2M_Y} (M_R - M_Y) \right\}^2 \right. \\ & \left. + 3 \left(g_1 - g_2 \frac{M_R}{2M_Y} \right)^2 (M_R - M_Y)^2 - 8g_2 M_R^2 \left(2g_1 - g_2 \frac{M_R}{2M_Y} \right) \right]. \quad (81) \end{aligned}$$

For $\mathcal{L}_{\gamma\Lambda\Lambda'}$, we use the data $\Gamma[\Lambda(1520) \rightarrow \Lambda\gamma]_{\text{expt.}} = 159 \pm 35 \text{ keV}$ [83] and set $g_2 = 0$ as in the case of $\Delta \rightarrow N\gamma$ to get

$$g_1 \approx 1.46. \quad (82)$$

For the photo-transitions of $\Lambda(1520)$ to other hyperons, we again are guided by the quark model predictions Ref. [78],

$$\begin{aligned} \Gamma[\Lambda(1520) \rightarrow \Sigma\gamma] &= 74 \text{ keV}, & \Gamma[\Lambda(1520) \rightarrow \Lambda(1405)\gamma] &= 0.2 \text{ keV}, \\ \Gamma[\Lambda(1520) \rightarrow \Sigma^*\gamma] &\sim 0. \end{aligned} \quad (83)$$

As the decay widths of $\Lambda(1520) \rightarrow \Sigma^*\gamma$ and $\Lambda(1405)\gamma$ are negligible, we only consider the coupling with the $\Sigma\gamma$ channel. Using $\Gamma[\Lambda(1520) \rightarrow \Sigma\gamma] = 74 \text{ keV}$ and also setting $g_2 = 0$, we get $\mathcal{L}_{\gamma\Sigma\Lambda'}$ with $g_1 \approx 1.39$.

With the above four subsections, we have constructed the Lagrangians for calculating all diagrams in Fig. 5. We now turn to discussing Θ production mechanisms.

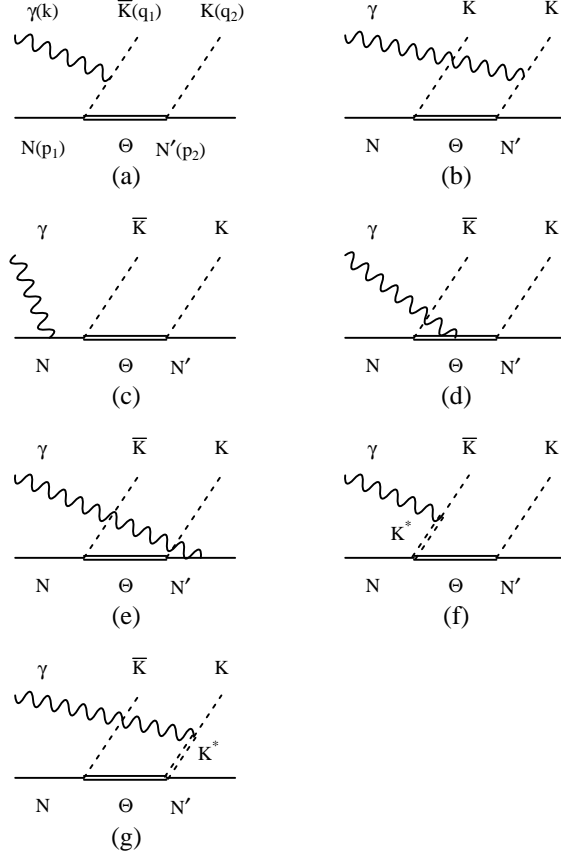


FIG. 6: Exotic $S = +1$ pentaquark Θ contribution to $\gamma N \rightarrow K\bar{K}N$.

E. Pentaquark contribution

The pentaquark $\Theta(1540)$ contribution to $\gamma N \rightarrow K\bar{K}N$ is depicted in Fig. 6. We first assume that it belongs to pentaquark baryon antidecuplet, which means that the $\Theta(1540)$ is an isosinglet state. In this case, $\Theta(1540)$ can contribute to, or can be observed in the reactions of $\gamma p \rightarrow K^0\bar{K}^0 p$ and $\gamma n \rightarrow K^+K^-n$. There is still no experimental clue on the existence of isovector Θ or isotensor Θ , which are members of pentaquark **27**-plet and **35**-plet, respectively. So we do not consider such cases and focus on the isosinglet Θ^+ since the nonexistence of a peak at 1540 MeV in K^+p channel strongly suggests the isosinglet nature of $\Theta(1540)$, if exists. Next we assume that $\Theta(1540)$ has spin-1/2 following most hadron model predictions. There may be its higher spin resonances, but it will not be investigated in this study. However, there are strong debates on the parity of $\Theta(1540)$. Therefore, in order to study the sensitivity of the physical quantities in $\gamma N \rightarrow K\bar{K}N$ on the parity of $\Theta(1540)$, we allow the both parities. Thus the effective Lagrangians are

$$\begin{aligned}
\mathcal{L}_{KN\Theta} &= -ig_{KN\Theta}\bar{\Theta}\Gamma^\pm\bar{K}^cN + \text{H.c.}, \\
\mathcal{L}_{K^*N\Theta} &= -g_{K^*N\Theta}\bar{\Theta}\left(\Gamma_\mu^\pm\bar{K}^{*c\mu} - \frac{\kappa_{K^*N\Theta}^T}{M_N + M_\Theta}\Gamma^\mp\sigma^{\mu\nu}\partial_\nu\bar{K}_\mu^{*c}\right)N + \text{H.c.}, \\
\mathcal{L}_{\gamma\Theta\Theta} &= -e\bar{\Theta}\left[A_\mu\gamma^\mu - \frac{\kappa_\Theta}{2M_N}\sigma_{\mu\nu}\partial^\nu A^\mu\right]\Theta,
\end{aligned} \tag{84}$$

where

$$\Gamma^\pm = \begin{pmatrix} \gamma_5 \\ 1 \end{pmatrix}, \quad \Gamma_\mu^\pm = \begin{pmatrix} \gamma_\mu \\ \gamma_\mu \gamma_5 \end{pmatrix}, \quad (85)$$

and

$$K^c = \begin{pmatrix} -\bar{K}^0 \\ K^- \end{pmatrix}, \quad K^{*c} = \begin{pmatrix} -\bar{K}^{*0} \\ K^{*-} \end{pmatrix}. \quad (86)$$

Here, the upper components of Γ^\pm and Γ_μ^\pm are for even-parity Θ^+ and the lower components for odd-parity Θ^- .

For the couplings of $\Theta(1540)$, we assume that $\Gamma(\Theta) = 1$ MeV [84], which is close to the value of Particle Data Group [59], 0.9 ± 0.3 MeV. We then have

$$g_{KN\Theta} = 0.984 \quad (0.137) \quad (87)$$

for positive (negative) parity Θ . There is no information about the $K^*N\Theta$ couplings. As in Ref. [46], we use $g_{K^*N\Theta}/g_{KN\Theta} = \sqrt{3}$ for even parity Θ and $g_{K^*N\Theta}/g_{KN\Theta} = 1/\sqrt{3}$ for odd parity Θ following the quark model predictions [39, 85, 86] while neglecting the tensor coupling terms. The dependence of our results on this ratio will be discussed later. As for the magnetic moment of $\Theta^+(1540)$, we use the prediction from Ref. [87], $\mu(\Theta) \approx 0.1$ (0.4), which gives $\kappa_\Theta \approx -0.9$ (-0.6). However, we found that our results are not sensitive to the value of κ_Θ .

III. RESULTS

Like all of the effective Lagrangian approaches, the considered tree-diagrams shown in the previous Section need to be regularized by introducing form factors. In this work, we use the form (28) which was already used in our investigation of tensor meson photoproduction in Section II.1. Namely, a form factor of the form of Eq. (28) is introduced at each vertex for all tree-diagrams in Section II, where M is the mass of the exchanged (off-shell) particle and r is its four-momentum squared. Therefore, when it is on its mass-shell ($r = M^2$), the form factor becomes 1.

It is well-known that introducing form factors breaks gauge invariance. In order to restore gauge invariance, we extend the methods of Refs. [32, 33, 34]. Namely, we introduce contact diagrams to restore the gauge invariance condition. The details on this procedure are given and discussed in Appendix B. For simplicity, we set the cutoff parameter Λ the same for all tree-diagrams and adjust it to fit the available experimental data of $\gamma N \rightarrow K\bar{K}N$ reactions. Obviously, it is not easy to interpret the resulting form factor theoretically. Rather it should be just considered as a part of our phenomenological approach.

A. Total cross sections

Since we assume that the $\Theta(1540)$ is a particle with isospin $I = 0$, strangeness $S = +1$ and charge $Q = +|e|$, the Θ production mechanisms (Fig. 6) can not take place in the $\gamma p \rightarrow K^+K^-p$ reaction. We thus determine the cutoff parameter Λ of the form factors by fitting the available total cross section data for $\gamma p \rightarrow K^+K^-p$. In this way the background (non- Θ mechanism) amplitude can be fixed, such that the identification of the Θ from the available data of $\gamma n \rightarrow K^+K^-n$ reaction can be assessed. With $\Lambda = 0.9$ GeV, our fit (solid

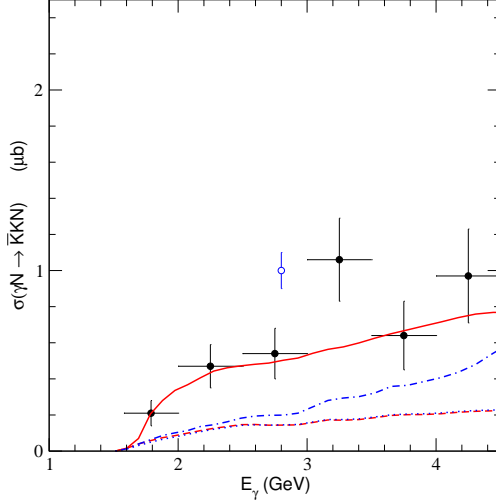


FIG. 7: Total cross sections for $\gamma N \rightarrow K\bar{K}N$ reactions. The solid line is for $\gamma p \rightarrow K^+K^-p$, dashed line for $\gamma p \rightarrow K^0\bar{K}^0p$, dot-dashed line for $\gamma n \rightarrow K^+K^-n$, and dotted line for $\gamma n \rightarrow K^0\bar{K}^0n$. The experimental data are for $\gamma p \rightarrow K^+K^-p$ reaction and from Ref. [88] (\bullet) and Ref. [89] (\circ). The dashed and dotted lines are close together and hard to be distinguished.

curve) is shown in Fig. 7. Clearly, the data can be reproduced reasonably well. With the same cutoff parameter, we then predict the total cross sections for the other three processes listed in Eq. (1). They are also shown in Fig. 7: $\gamma p \rightarrow K^0\bar{K}^0p$ (dashed line), $\gamma n \rightarrow K^+K^-n$ (dot-dashed line), and $\gamma n \rightarrow K^0\bar{K}^0n$ (dotted line). We can see that the cross sections for neutral $K^0\bar{K}^0$ pair photoproduction from p (dashed curve) or n (dotted curve) are almost indistinguishable, and the cross sections for charged K^+K^- pair photoproduction (solid and dash-dot curves) are larger than those for neutral $K^0\bar{K}^0$ pair production. The contributions from the $\Theta(1540)$ are not visible in the calculated total cross sections. The Θ can be identified only in the invariant mass distributions.

B. Invariant mass distributions

With the cutoff $\Lambda = 0.9$ GeV determined from the total cross section for the $\gamma p \rightarrow K^+K^-p$ reaction, we can now compare our predictions of the invariant mass distributions for the $\gamma n \rightarrow K^+K^-n$ reaction with the JLab data [3]. Unfortunately, the JLab data are not scaled properly for comparing with the absolute magnitudes of the predicted cross sections. We therefore simply scale the JLab data to see whether we can roughly reproduce the shape of the data within our model.⁸ This must be a very crude assumption but will be enough to study the shape, especially the Θ peak, of the data.

The results from assuming an even-parity (odd-parity) $\Theta(1540)$ are presented in Fig. 8 (Fig. 9) at $E_\gamma = 2.3$ GeV. In both cases, we can reproduce very well the ϕ peak of the

⁸ It should also be mentioned that the JLab data were not obtained with a single photon energy, instead the data were taken by incident electrons of 2.474 and 3.115 GeV, and the nuclear effects are not properly taken into account.

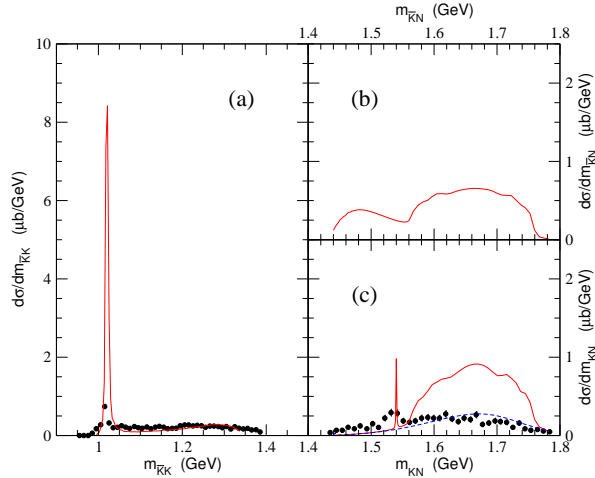


FIG. 8: (a) K^+K^- , (b) K^-N , and (c) K^+N invariant mass distributions for $\gamma n \rightarrow K^+K^-n$ at $E_\gamma = 2.3$ GeV. The experimental data are from Refs. [3]. The dashed line in (c) is obtained without the ϕ meson background and the Θ contributions. Here we assume that the $\Theta(1540)$ has even parity.

K^+K^- mass distributions [Fig. 8(a) and Fig. 9(a)]. The predicted shape in other region of the K^+K^- invariant mass also qualitatively agrees with the data.

The comparisons with the data of the K^+n mass distributions are shown in Fig. 8(c) and Fig. 9(c). Note that the JLab data were obtained from removing the $\phi \rightarrow K^+K^-$ decay contributions at the ϕ peak and hence should only be compared with the dashed curves which are obtained from turning off the ϕ and Θ production contribution in our calculations.⁹ For completeness, our full predictions (solid curves) are also displayed in (c) of Fig. 8 and Fig. 9. We see that the peak in K^+N mass distribution arising from the production of the $\Theta(1540)$ is not so much pronounced as in the case of the ϕ meson peak in K^+K^- invariant mass distribution. This is mainly due to the small coupling of the Θ with K^+N and K^*N . We also observe in Fig. 9(c) that the $\Theta(1540)$ peak is much smaller in the case of odd-parity Θ . Shown in (b) of Figs. 8 and 9 are the K^-n mass distribution.

By comparing the dashed curves and the experimental data in Fig. 8(c) and Fig. 9(c), we can see that the shape of the data can be reproduced well by our model except in the region near the $\Theta(1540)$ peak. The width of the peak cannot be simply judged since the broad width of the JLab data shows the detector resolution. Besides, there are two possible interpretations of our results. First, the $\Theta(1540)$ is produced and the discrepancy between the data and the obtained curves is due to the low statistics of the experiment. On the other hand, the discrepancy is perhaps due to the deficiency of our model in accounting for other possible non- Θ mechanisms and the existence of Θ is questionable. As discussed in the previous Sections, we are limited by the lack of information in calculating some allowed non- Θ background mechanisms. Obviously, high statistics and high resolution experiments are strongly required. The existence of $\Theta(1540)$ can be unambiguously established if and

⁹ We turn off the Θ contribution in the dashed curves in Fig. 8(c) and Fig. 9(c) in order to show the enhancement of the Θ peak compared with the backgrounds.

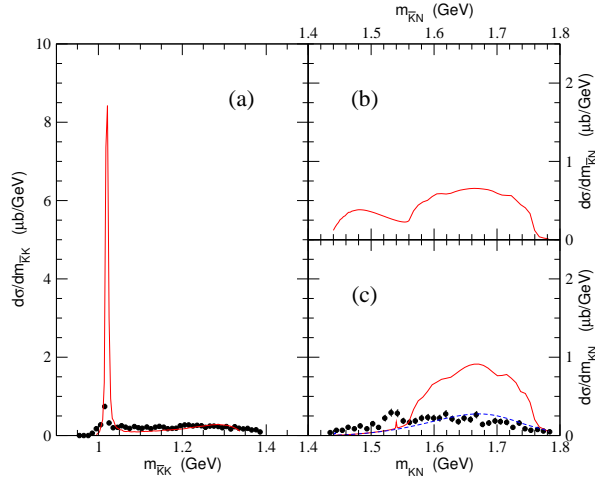


FIG. 9: (a) $K\bar{K}$, (b) $\bar{K}N$, and (c) KN invariant mass distributions for $\gamma n \rightarrow K^+K^-n$ at $E_\gamma = 2.3$ GeV. The experimental data are from Refs. [3]. Notations are the same as in Fig. 8. Here we assume that the $\Theta(1540)$ has odd parity.

only if a very sharp resonance peak, which is very unlikely due to the background amplitudes as predicted by our model, is observed. Furthermore, an even-parity Θ is more likely to be detected, while it will be difficult to identify an odd-parity Θ , even if it exists, from the background continuum. This is because the odd-parity Θ has much smaller couplings with the KN channel than the even-parity Θ when the same decay width is assigned. Therefore, if the observed $\Theta(1540)$ has odd-parity, it must have larger decay width, at least, one order of magnitude larger than the current estimate in Ref. [59] or it should have a large coupling to the other channels [31].

To facilitate the future experimental searches, we now present our predictions for the other three processes listed in Eq. (1). In Fig. 10, we give the results for the $\gamma p \rightarrow K^+K^-p$ reaction at $E_\gamma = 2.3$ GeV. Since we assume that $\Theta(1540)$ is isoscalar and can not contribute to this reaction, there is no peak in K^+p mass distribution. The peak in Fig. 10(b) of the K^-p mass distribution is due to the $\Lambda(1520)$ of hyperon background (Fig. 5). The dashed line in Fig. 10(c) is obtained when the contributions from the ϕ and $\Lambda(1520)$ are neglected in the calculation. Clearly, these two mechanisms are the major background production processes. Experimental test of our predictions presented in Fig. 10 will also be an important task to check our model of non- Θ background mechanisms which must be understood before the predictions for $\gamma n \rightarrow K^+K^-n$ can be used to determine the existence of the $\Theta(1540)$.

The results for $\gamma p \rightarrow K^0\bar{K}^0p$ are shown in Figs. 11 and 12 for the even and odd parity Θ , respectively. We see that the $\Theta(1540)$ peak in Fig. 11 is much smaller than that in the $\gamma n \rightarrow K^+K^-n$ reaction (Fig. 8). The peak from the odd-parity $\Theta(1540)$ is hardly to be seen in the KN invariant mass distribution in $\gamma p \rightarrow K^0\bar{K}^0p$ as shown in Fig. 12.

The results for $\gamma n \rightarrow K^0\bar{K}^0n$ are given in Fig. 13. Again, there is no contribution from the isoscalar Θ to this reaction and therefore there is no peak in the KN invariant mass distribution [Fig. 13(c)]. Here we also find that the predicted cross sections [dashed curve in Fig. 13(c)] is greatly reduced if the contributions from the ϕ and $\Lambda(1520)$ productions are

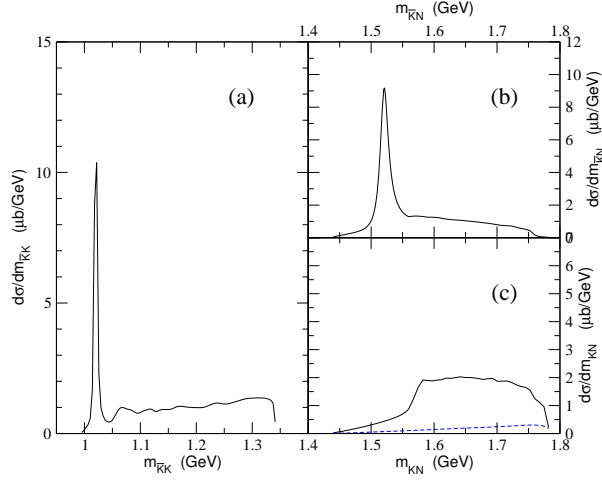


FIG. 10: (a) $K\bar{K}$, (b) $\bar{K}N$, and (c) KN invariant mass distributions for $\gamma p \rightarrow K^+K^-p$ at $E_\gamma = 2.3$ GeV. The dashed line in (c) is obtained without the ϕ meson background and the $\Lambda(1520)$ contribution.

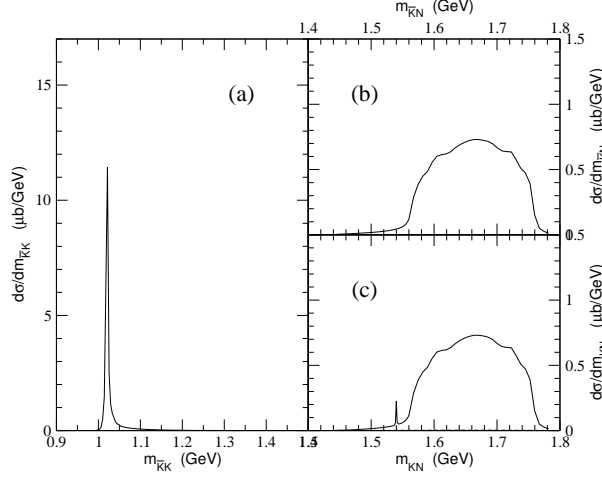


FIG. 11: (a) $K\bar{K}$, (b) $\bar{K}N$, and (c) KN invariant mass distributions for $\gamma p \rightarrow K^0\bar{K}^0p$ at $E_\gamma = 2.3$ GeV. The dashed line in (c) is obtained without the ϕ meson background and the $\Theta(1540)$ contribution and magnified by a factor of 10. Here we assume that the $\Theta(1540)$ has even parity.

turned off.

C. Tensor meson photoproduction contributions

In this subsection, we discuss in more detail the contribution of the tensor meson production to the $\gamma n \rightarrow K^+K^-n$ reaction, which is an important issue raised by Dzierba *et al.* [26],

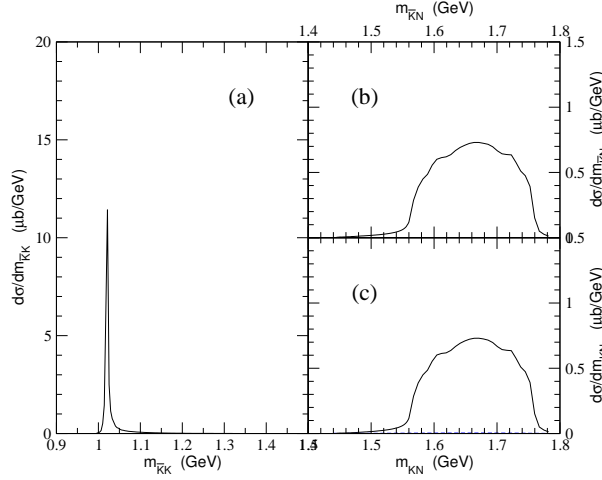


FIG. 12: (a) $K\bar{K}$, (b) $\bar{K}N$, and (c) KN invariant mass distributions for $\gamma p \rightarrow K^0\bar{K}^0 p$ at $E_\gamma = 2.3$ GeV. The dashed line in (c) is obtained without the ϕ meson background and the $\Theta(1540)$ contribution and magnified by a factor of 10. Here we assume that the $\Theta(1540)$ has odd parity. Since the contribution from $\Theta(1540)$ is suppressed, its peak is not seen in (c).

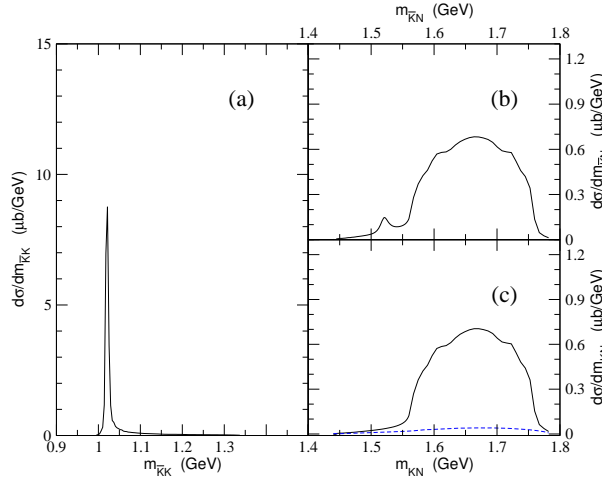


FIG. 13: (a) $K\bar{K}$, (b) $\bar{K}N$, and (c) KN invariant mass distributions for $\gamma n \rightarrow K^0\bar{K}^0 n$ at $E_\gamma = 2.3$ GeV. The dashed line in (c) is obtained without the ϕ meson background and the $\Lambda(1520)$ contribution.

who indicated the possibility that the observed peak at 1540 MeV in the KN invariant mass distribution could be a false peak arising from tensor meson background. Their calculation of neutral tensor meson photoproduction is based on a model of pion trajectory exchange mechanism. However, as we discussed in Section II, the pion exchange is not allowed for this process because of the C parity, and the lowest allowed exchanged particles are vector mesons. Although the production mechanism used by the authors of Ref. [26] is questionable,

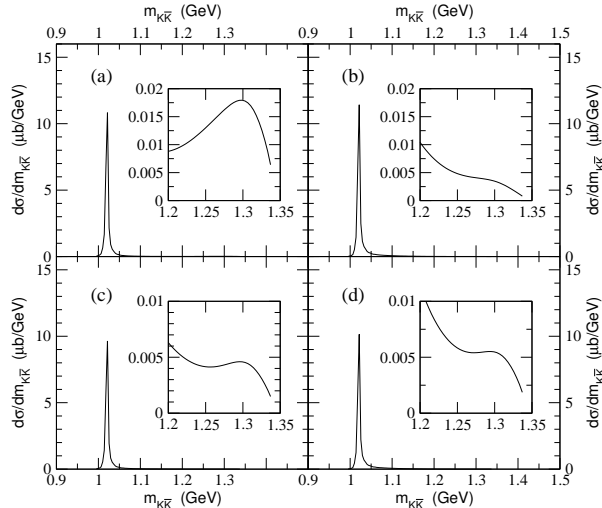


FIG. 14: Vector meson and tensor meson contributions to $K\bar{K}$ invariant mass distributions for (a) $\gamma p \rightarrow K^+K^-p$, (b) $\gamma p \rightarrow K^0\bar{K}^0p$, (c) $\gamma n \rightarrow K^+K^-n$, (d) $\gamma n \rightarrow K^0\bar{K}^0n$ at $E_\gamma = 2.3$ GeV. Shown in the small windows are the region of tensor meson peaks.

their claim should be checked by a calculation using the vector meson exchange mechanism, as formulated in Section II.2.B.

Our calculations of the vector meson and tensor meson contributions to the $K\bar{K}$ mass distributions of the four processes listed in Eq. (1) are displayed in Fig. 14. The contributions from tensor mesons (displayed in small windows of Fig. 14) are clearly much smaller than the vector meson contributions. Furthermore, because of their large decay widths, $\Gamma(f_2(1275)) \approx 185$ MeV and $\Gamma(a_2(1320)) \approx 107$ MeV, the contributions from these two tensor mesons do not give distinguishable two peaks in $K\bar{K}$ mass distribution. We also note that the tensor meson peak in $\gamma p \rightarrow K^+K^-p$ reaction is much more pronounced than in the other reactions. This is due to the isospin factors associated with the coupling constants, which define the relative phases between different contributions in each process. As seen in Table III, the resulting relative phases lead to constructive interference in $\gamma p \rightarrow K^+K^-p$ reaction and destructive interference in the other reactions. As a result, the tensor meson peaks in the $\gamma n \rightarrow K^+K^-n$ reaction is smaller than those in the $\gamma p \rightarrow K^+K^-p$ reaction. Therefore, the claim raised by Ref. [26] can be checked by comparing the results from the above two reactions. Namely, if the peak at 1540 MeV in the $\gamma n \rightarrow K^+K^-n$ reaction is coming from the tensor meson contribution, one could expect a similar or even much clear peak at around 1540 MeV in $\gamma p \rightarrow K^+K^-p$ reaction with the similar energy of the photon beam. The absence of such a peak in $\gamma p \rightarrow K^+K^-p$ reported by the SAPHIR [4] and HERMES [7] Collaborations, therefore, seems to disfavor the possibility of ascribing the peak at 1540 MeV in the KN mass distribution of $\gamma n \rightarrow K^+K^-n$ to the tensor meson background. This, of course, should be further examined by other higher statistics experiments.

In Fig. 15, we give our results for KN invariant mass distribution coming solely from the tensor meson photoproduction part. Although their maximal values locate at around 1.56 GeV at $E_\gamma = 2.3$ GeV (solid curve), the shapes are very broad and most of the magnitudes are much smaller than the other backgrounds by about two orders of magnitude. Thus, the tensor meson contributions estimated within our model based on vector meson exchange

Reaction	a_2^0 photoproduction			f_2^0 photoproduction		
	ω exchange	ρ exchange	$a_2^0 \rightarrow K\bar{K}$	ω exchange	ρ exchange	$f_2^0 \rightarrow K\bar{K}$
$\gamma p \rightarrow K^+ K^- p$	+	+	+	+	+	+
$\gamma p \rightarrow K^0 \bar{K}^0 p$	+	+	-	+	+	+
$\gamma n \rightarrow K^+ K^- n$	+	-	+	+	-	+
$\gamma n \rightarrow K^0 \bar{K}^0 n$	+	-	-	+	-	+

TABLE III: Relative phases of tensor meson photoproduction contribution to the $\gamma N \rightarrow K\bar{K}N$ reaction.

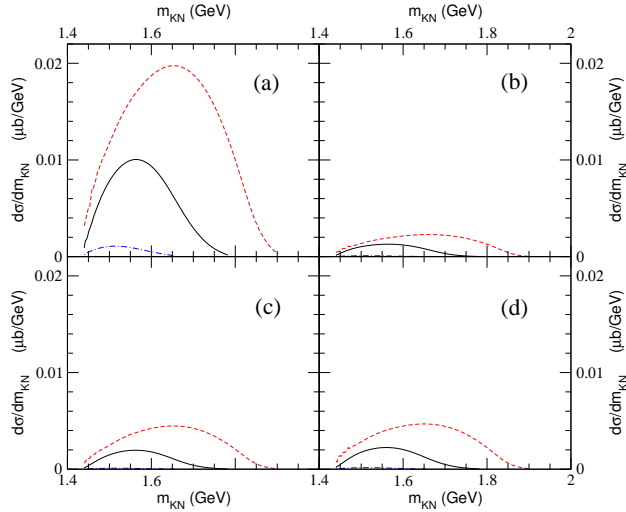


FIG. 15: Tensor meson contribution to KN invariant mass distributions for (a) $\gamma p \rightarrow K^+ K^- p$, (b) $\gamma p \rightarrow K^0 \bar{K}^0 p$, (c) $\gamma n \rightarrow K^+ K^- n$, (d) $\gamma n \rightarrow K^0 \bar{K}^0 n$ at $E_\gamma = 2.3$ GeV. The dot-dashed, solid, and dashed lines are at $E_\gamma = 2.0, 2.3,$ and 2.6 GeV, respectively. The dot-dashed lines in (b,c,d) are suppressed and hard to be seen within the given scale.

are too weak to generate any narrow peak in the presence of other much larger background processes even if the ϕ meson background is removed. We therefore conclude that we could not verify the claim of Ref. [26]. Our results also show that, if the peak is from the tensor meson background, its position should change with different photon beam energies.

D. Double differential cross sections and spin asymmetries

The double differential cross sections and the spin asymmetries are calculated for the three cases; no pentaquark, even-parity $\Theta(1540)$, and odd-parity $\Theta(1540)$. Since we are interested in the existence and parity of isoscalar Θ , we now focus on the $\gamma n \rightarrow K^+ K^- n$ reaction, which has larger cross sections than $\gamma p \rightarrow K^0 \bar{K}^0 p$. As discussed in Refs. [51, 52, 53], we have model-dependence on the spin asymmetries in most reactions, except the NN reaction near the threshold. Therefore, we do not make a definite conclusion on the dependence of spin asymmetries on the parity of Θ . Instead, we present the results of our model and mention about the possible resonance structure in the energy dependence of some spin asymmetries.

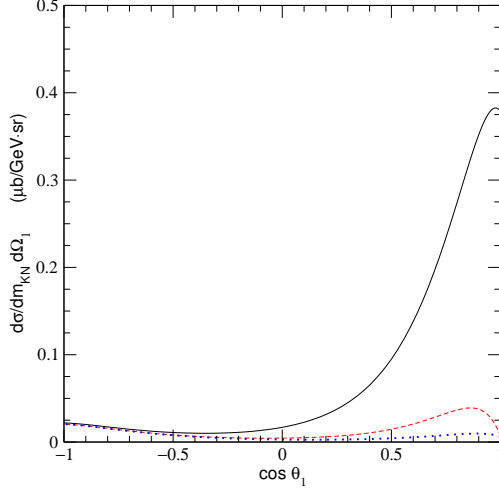


FIG. 16: Double differential cross section $d\sigma/dm_{KN}d\Omega_1$ as a function of $\cos\theta_1$, where θ_1 is the polar angle of K^- in the center of mass frame, for $\gamma n \rightarrow K^+K^-n$ with $E_\gamma = 2.3$ GeV and $m_{KN} = 1.54$ GeV. The dotted line is obtained without $\Theta(1540)$, while the solid (dashed) line is with even (odd) parity of Θ .

In this work, we compute two spin asymmetries, single photon beam asymmetry and beam-target double asymmetry.

Shown in Fig. 16 is the double differential cross sections for the $\gamma n \rightarrow K^+K^-n$ reaction at $E_\gamma = 2.3$ GeV and $m_{KN} = 1.54$ GeV, i.e., at the resonance point, as a function of $\cos\theta_1$, where θ_1 is the polar angle of K^- in the γN center of mass frame of which z axis is defined as the photon beam direction. Figure 17 shows the photon beam asymmetry Σ_x and beam-target double asymmetry C_{BT} for the $\gamma n \rightarrow K^+K^-n$ reaction at $E_\gamma = 2.3$ GeV and $m_{KN} = 1.54$ GeV. They are defined as

$$\Sigma_x = \frac{d\sigma^\parallel - d\sigma^\perp}{d\sigma^\parallel + d\sigma^\perp}, \quad (88)$$

where $d\sigma^\parallel$ ($d\sigma^\perp$) corresponds the differential cross sections due to a photon linearly polarized along the \hat{x} (\hat{y}) axis, and

$$C_{BT} = \frac{d\sigma^{\uparrow\uparrow} - d\sigma^{\downarrow\downarrow}}{d\sigma^{\uparrow\uparrow} + d\sigma^{\downarrow\downarrow}}, \quad (89)$$

where $d\sigma^{\uparrow\uparrow}$ and $d\sigma^{\downarrow\downarrow}$ represent the differential cross sections when the photon and target helicities are parallel and anti-parallel, respectively. In these figures, the solid lines are for even-parity Θ and the dashed lines are for odd-parity Θ . The dotted lines are for the background, i.e., without Θ . Our results show that the differential cross sections are enhanced by the presence of even-parity Θ in the forward scattering region of K^- meson direction. This suggests that the kinematic cut for the angle of K^- would be useful to enhance the Θ peak in KN mass distributions. But for the odd-parity Θ , this enhancement is small. This difference is primarily due to the magnitude of the Θ couplings. The considered asymmetries, the photon beam asymmetry and beam-target double asymmetry, are rather sensitive to the parity of the $\Theta(1540)$. But in the case of beam-target double asymmetry, the difference between the odd-parity Θ (dashed line) and the background processes (dotted line) is not large. Although the model-dependence is unavoidable, our model calculation

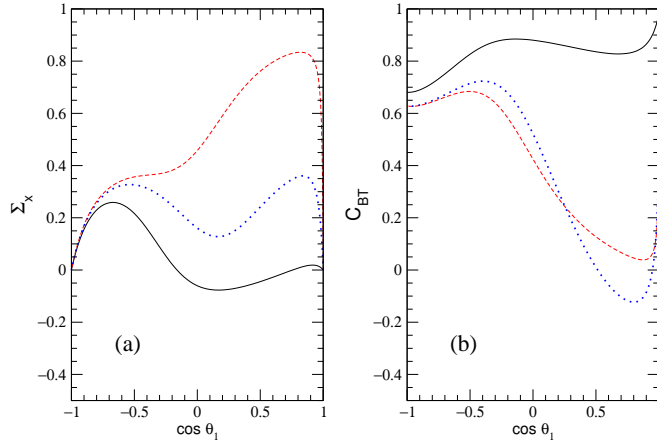


FIG. 17: (a) Photon beam asymmetry Σ_x and (b) beam-target double asymmetry C_{BT} as a function of $\cos \theta_1$ for $\gamma n \rightarrow K^+K^-n$ with $E_\gamma = 2.3$ GeV and $m_{KN} = 1.54$ GeV. Notations are the same as in Fig. 16.

shows that these spin asymmetries can be used to explore the parity of $\Theta(1540)$, especially in the forward scattering region. (See the discussions below.)

In Fig. 18, we show the photon beam asymmetries at $\theta_1 = 30^\circ$ and the beam-target double asymmetry at $\theta_1 = 0^\circ$ as functions of m_{KN} at $E_\gamma = 2.3$ GeV. This clearly shows the resonance structure in these asymmetries when the Θ has even parity. For odd-parity Θ , as can be seen from Fig. 16, its contribution is small and the resonance structure in the beam-target double asymmetry is not manifest. Thus, although the parity of $\Theta(1540)$ may not be uniquely determined by these asymmetries because of model-dependence [51], our results strongly suggests a resonance structure in the asymmetries.

Here we note that the present results on the photon beam asymmetry agree qualitatively with the earlier results of Ref. [28] obtained within a much simpler model. Although the numerical values and the structure at large K^- angles are different, these two models are consistent at least qualitatively at forward angles of the K^- momentum in the center of mass frame.¹⁰ In Ref. [31], it is claimed that the single and double spin asymmetries are not sensitive to the parity of the $\Theta(1540)$. We found that this comes mainly from the role of the K^* exchanges, Fig. 6(f,g). In Ref. [31], the authors used the signal to background ratio to constrain the ratio $\alpha \equiv g_{K^*N\Theta}/g_{KN\Theta}$, which leads to $\alpha = 1.875$ and 8.625 for the even and odd parity Θ . (Note that α for the odd parity Θ is much larger than the quark model prediction by a factor of 15.) As a consequence, they have the K^* -exchange dominance in the Θ production mechanism especially in the case of odd-parity Θ , and as a result the single and double asymmetries are not sensitive to the parity of Θ . In our calculation we used $\alpha = \sqrt{3}$ and $1/\sqrt{3}$ for the even and odd parity Θ following the quark model predictions. If we use the α values of Ref. [31], we could verify that the sensitivity of the asymmetries on the Θ parity becomes weak. We also found that the spin asymmetries are sensitive to the parity of Θ is $\alpha < 1$ for the odd parity Θ . Therefore, this illustrates the model-dependence

¹⁰ Note also that our Σ_x corresponds to $-\Sigma$ of Ref. [28].

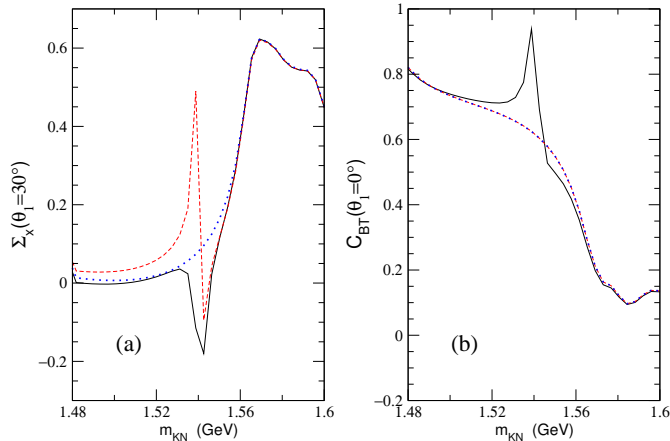


FIG. 18: (a) Single photon beam asymmetry at $\theta_1 = 30^\circ$ and (b) beam-target double asymmetry C_{BT} at $\theta_1 = 0^\circ$ as functions of m_{KN} for $\gamma n \rightarrow K^+ K^- n$ at $E_\gamma = 2.3$ GeV. Notations are the same as in Fig. 16.

of the asymmetries and it is very important to estimate the correct order of magnitude of α , which is, however, not possible at the present state.

IV. SUMMARY

In this work, we have investigated how the $\gamma N \rightarrow K\bar{K}N$ reaction can be used to study the production and the properties of the pentaquark $\Theta(1540)$ baryon. We study the case that $\Theta(1540)$ is a spin $J = 1/2$ and isospin $I = 0$ particle, and have focused on the influence of the background (non- Θ) amplitudes due to the Drell diagrams (Fig. 1), the $K\bar{K}$ production through the intermediate vector meson and tensor meson photoproduction (Fig. 2), and the mechanisms involving intermediate $\Lambda(1116)$, $\Lambda(1405)$, $\Lambda(1520)$, $\Sigma(1193)$, $\Sigma(1385)$, and $\Delta(1232)$ states (Fig. 5). The vector meson photoproduction amplitude is calculated from a phenomenological model which describes well the experimental data at low energies. The charged tensor meson production amplitude is calculated from a one-pion-exchange model, which describes well the total cross section data of $\gamma p \rightarrow a_2^+(1320)n$. The neutral tensor meson production part is estimated by using the vector meson exchange mechanisms. The coupling constants needed for calculating all of the considered background mechanisms are deduced from the data of decay widths by imposing the SU(3) symmetry or making use of various quark model predictions. No attempt is made to calculate other background amplitudes which are kinematically allowed but can not be computed because of the lack of experimental information. Thus the present work represents only a step toward a complete dynamical description of the $\gamma N \rightarrow K\bar{K}N$ reaction. Nevertheless, some progress has been made in assessing the existing data concerning the existence of the $\Theta(1540)$ pentaquark state.

The $\Theta(1540)$ production mechanism (Fig. 6) is calculated by taking 1 MeV as its decay width, which is close to the Particle Data Group value. With the background amplitude constrained by the total cross section data of $\gamma p \rightarrow K^+ K^- p$ (the considered isoscalar $\Theta(1540)$

is not allowed in the process), we find that the resulting K^+K^- and K^+n invariant mass distributions of the $\gamma n \rightarrow K^+K^-n$ reaction can qualitatively reproduce the shapes of the JLab data. However, the predicted $\Theta(1540)$ peak can not be identified unambiguously with the data. There are two possible interpretations of our results. First, it is possible that the $\Theta(1540)$ is produced and the discrepancy between the data and our results is due to the low statistics of the experiment. On the other hand, the discrepancy is perhaps due to the deficiency of our model in accounting for other possible non- Θ mechanisms and the existence of $\Theta(1540)$ is questionable. Obviously, high statistics and high resolution experiments are needed. The existence of $\Theta(1540)$ can be unambiguously established if and only if a very sharp resonance peak, which is very unlikely from the background amplitudes as predicted by our model, is observed. We also find that an even-parity Θ is more likely to be detected, while it will be difficult to identify an odd-parity Θ , even if it exists, from the background continuum, unless it has much larger coupling to the K^*N channel than the current quark model predictions.

We have analyzed in some detail the contributions of the tensor meson to $\gamma n \rightarrow K^+K^-n$ reaction, which is an important issue raised by Dzierba *et al.* [26]. (See also Ref. [90].) These authors indicated that the observed peak at 1540 MeV in the KN invariant mass distribution could be a false peak arising from tensor meson background. What we found are (1) the calculation of Ref. [26] is based on the π^0 exchange mechanism which can not take place in neutral tensor meson photoproduction if the C -parity is conserved. (2) Instead of π^0 exchange, we estimate the neutral tensor meson contributions by using the vector meson exchange model, and have found that the neutral tensor meson contribution is too weak to generate any resonance peaks which can be identified with the existing data of $\gamma n \rightarrow K^+K^-n$ reaction.

Finally, we also show that the photon beam asymmetry and the beam-target double asymmetry can be useful to help confirm the existence of $\Theta(1540)$ and determine its parity. Here the major uncertainty comes from the ratio $\alpha \equiv g_{K^*N\Theta}/g_{KN\Theta}$, and our results are obtained with the assumption that $\alpha < 1$ for negative parity $\Theta(1540)$ as in the present quark model predictions. Those observables can be measured at current experimental facilities.

Acknowledgments

We are grateful to K. Hicks, K. Joo, T. Nakano, and A.I. Titov for useful information and fruitful discussions. We also thank V. Burkert for valuable comments. Y.O. acknowledges fruitful discussions with Hungchong Kim. This work was supported by Forschungszentrum-Jülich, contract No. 41445282 (COSY-058) and U.S. DOE Nuclear Physics Division Contract No. W-31-109-ENG-38.

APPENDIX A: TENSOR MESONS

In this Appendix, we discuss the couplings of tensor mesons to hadrons and their radiative decays. Among the spin-2 tensor mesons, we are interested in $f_2(1270)$, $f'_2(1525)$, and $a_2(1320)$ as they can decay into two kaons and close to the threshold energy region of the

$\gamma N \rightarrow K\bar{K}N$ reaction.¹¹ The $f_2(1270)$ and $f'_2(1525)$ have the quantum numbers $I^G(J^{PC}) = 0^+(2^{++})$. The $f_2(1270)$ has mass $M_{f_2} = 1275$ MeV, width $\Gamma_{f_2} = 185.1$ MeV, and it mostly decays into two pions. Some of its branching ratios are $\text{BR}(f_2 \rightarrow \pi\pi) = (84.7^{+2.4}_{-1.3})\%$, $\text{BR}(f_2 \rightarrow K\bar{K}) = (4.6 \pm 0.5)\%$, and $\text{BR}(f_2 \rightarrow \gamma\gamma) = (1.41 \pm 0.13) \times 10^{-5}$.

The $f'_2(1525)$ has $M_{f'_2} = 1525$ MeV and $\Gamma_{f'_2} = 76 \pm 10$ MeV. It mostly decays into two kaons and some of its branching ratios are $\text{BR}(f'_2 \rightarrow K\bar{K}) = (88.8 \pm 3.1)\%$ and $\text{BR}(f'_2 \rightarrow \gamma\gamma) = (1.23 \pm 0.17) \times 10^{-6}$.

The $a_2(1320)$ is an isovector tensor meson with $M_{a_2} = 1318$ MeV and $\Gamma_{a_2} = 107 \pm 5$ MeV. It mostly decays into $\rho\pi$, but it decays also into two kaons, $\pi\gamma$, and two photons with $\text{BR}(a_2 \rightarrow K\bar{K}) = (4.9 \pm 0.8)\%$, $\text{BR}(a_2 \rightarrow \pi^\pm\gamma) = (2.68 \pm 0.31) \times 10^{-3}$, and $\text{BR}(a_2 \rightarrow \gamma\gamma) = (9.4 \pm 0.7) \times 10^{-6}$. Note that $a_2^0 \rightarrow \pi^0\gamma$ decay is not allowed because of C -parity. By the same reason, $f_2 \rightarrow \pi^0\gamma$ is forbidden.

In our calculation, we use the coupling constants determined from the experimental data and quark model predictions. Here, we discuss the way to determine the couplings and compare the values with those obtained by assuming SU(3) symmetry and vector meson dominance.

1. Interactions with pseudoscalar mesons

Since f_2 and a_2 are spin-2 tensor mesons, we are dealing with tensor meson nonet whose members are $a_2(1320)$, $K_2(1430)$, $f_2(1275)$, and $f'_2(1525)$. This is analogous to vector meson nonet of ρ , K^* , ω , and ϕ .

The pseudoscalar octet is represented by an SU(3) matrix P which is defined in Eq. (6). Similarly, the tensor meson octet is represented by T_8 as

$$T_8 = \begin{pmatrix} \frac{1}{\sqrt{6}}f_8 + \frac{1}{\sqrt{2}}a_2 & K_2 \\ \bar{K}_2 & -\frac{2}{\sqrt{6}}f_8 \end{pmatrix}, \quad (\text{A1})$$

where $a_2 = \mathbf{a}_2 \cdot \boldsymbol{\tau}$. The Lorentz index $\mu\nu$ is suppressed. Then the $T_8 PP$ interaction is obtained as

$$\mathcal{L} = g\text{Tr} (T_8^{\mu\nu} \partial_\mu P \partial_\nu P), \quad (\text{A2})$$

which gives the SU(3) symmetry relations to the coupling constants.

Since $f_2(1275)$ and $f'_2(1525)$ are expected to be close to ideal mixing, we introduce the tensor meson singlet f_0 , whose interaction with two pseudoscalar mesons is given by

$$\begin{aligned} \mathcal{L}_{f_0 PP} &= \frac{g}{\sqrt{3}}\text{Tr} (f_0^{\mu\nu} \partial_\mu P \partial_\nu P) \\ &= \frac{g}{\sqrt{3}}f_0^{\mu\nu} \{ \partial_\mu \eta \partial_\nu \eta + \partial_\mu \boldsymbol{\pi} \cdot \partial_\nu \boldsymbol{\pi} + 2\partial_\mu \bar{K} \partial_\nu K \}. \end{aligned} \quad (\text{A3})$$

Now we consider the mixing of f_8 and f_0 . The physical states f_2 and f'_2 are written as

$$\begin{aligned} f' &= \cos\theta f_8 - \sin\theta f_0, \\ f &= \sin\theta f_8 + \cos\theta f_0, \end{aligned} \quad (\text{A4})$$

¹¹ The $f'_2(1525)$, which mostly decays into $K\bar{K}$, is expected to be in $s\bar{s}$ state. Therefore, its coupling to the nucleon would be suppressed. Because of its higher mass and assuming the OZI rule as the first approximation, we do not include f'_2 photoproduction in our study of $K\bar{K}$ photoproduction processes.

where f_2 and f'_2 are denoted by f and f' , respectively. Then we have

$$\begin{aligned} g_{f'\pi\pi} &= \frac{g}{\sqrt{3}} \left(\frac{1}{\sqrt{2}} \cos \theta - \sin \theta \right), & g_{f\pi\pi} &= \frac{g}{\sqrt{3}} \left(\frac{1}{\sqrt{2}} \sin \theta + \cos \theta \right), \\ g_{f'KK} &= -\frac{g}{\sqrt{3}} \left(\frac{1}{\sqrt{2}} \cos \theta + 2 \sin \theta \right), & g_{fKK} &= \frac{g}{\sqrt{3}} \left(-\frac{1}{\sqrt{2}} \sin \theta + 2 \cos \theta \right). \end{aligned} \quad (\text{A5})$$

The mixing angle can be estimated from the masses of tensor meson nonet;

$$\tan^2 \theta = \frac{3M_{f'}^2 - 4M_{K_2}^2 + M_{a_2}^2}{4M_{K_2}^2 - M_{a_2}^2 - 3M_f^2} \approx 0.35, \quad (\text{A6})$$

where we have used the Gell-Mann–Okubo mass relation for squared masses of tensor mesons. This gives us

$$\theta \approx 30.5^\circ, \quad (\text{A7})$$

where the ideal mixing angle is $\theta_{\text{idealmixing}} \approx 35.3^\circ$. Note that in the case of vector meson nonet, the mixing angle is $\theta_V \approx 40^\circ$. Therefore, we can see that the tensor meson nonet is as close to ideal mixing as the vector meson nonet.¹²

The $2^+0^-0^-$ interaction is obtained as

$$\mathcal{L} = -\frac{2G_{f\pi\pi}}{M_f} \partial_\mu \boldsymbol{\pi} \cdot \partial_\nu \boldsymbol{\pi} f^{\mu\nu}, \quad (\text{A8})$$

which gives the decay width of $f_2 \rightarrow \pi\pi$ as

$$\Gamma(f_2 \rightarrow \pi\pi) = \frac{2}{5\pi} \frac{G_{f\pi\pi}^2}{M_f^4} p_F^5, \quad (\text{A9})$$

where $p_F = M_f \sqrt{1/4 - M_\pi^2/M_f^2}$. Using $\Gamma(f_2 \rightarrow \pi\pi)_{\text{expt.}} \approx 156.9 \text{ MeV}$ and $\Gamma(f'_2 \rightarrow \pi\pi)_{\text{expt.}} \approx 0.623 \text{ MeV}$, we obtain

$$G_{f\pi\pi} = 5.76, \quad G_{f'\pi\pi} = 0.33 = 0.06 G_{f\pi\pi}. \quad (\text{A10})$$

Similarly, $f \rightarrow K\bar{K}$ vertex can be obtained from

$$\mathcal{L} = -\frac{2G_{fKK}}{M_f} \partial_\mu \bar{K} \partial_\nu K f^{\mu\nu}. \quad (\text{A11})$$

Thus the decay width $f_2 \rightarrow K\bar{K}$ is estimated as

$$\Gamma(f_2 \rightarrow K\bar{K}) = \frac{2}{15\pi} \frac{G_{fKK}^2}{M_f^4} p_F^5, \quad (\text{A12})$$

which gives

$$G_{fKK} = 7.15 = 1.24 G_{f\pi\pi}. \quad (\text{A13})$$

¹² Note that we are assuming $q\bar{q}$ structure of the tensor meson, which may contain non-negligible glueball component.

with $\Gamma(f_2 \rightarrow K\bar{K})_{\text{expt.}} \approx 8.6 \pm 0.8$ MeV. This expression can also be applied to $f'_2(1525)$ meson decay, and with $\Gamma(f'_2 \rightarrow K\bar{K})_{\text{expt.}} \approx 65 \pm 5$ MeV we get

$$G_{f'KK} = -11.23 = -1.95G_{f\pi\pi}, \quad (\text{A14})$$

where the interaction is given by

$$\mathcal{L} = -\frac{2G_{f'KK}}{M_{f'}} \partial_\mu \bar{K} \partial_\nu K f'^{\mu\nu}. \quad (\text{A15})$$

Note that f_2 and f'_2 has the same quantum number and they are anticipated to form ideal mixing as in the case for ω and ϕ mesons. This is because f_2 mostly decays into two pions, while f'_2 mostly into two kaons. But the presence of $f_2 \rightarrow K\bar{K}$ decay implies the deviation from the ideal mixing.

In the case of $a_2(1320)$, because of its isovector nature, the interaction Lagrangian reads

$$\mathcal{L} = -\frac{2G_{aKK}}{M_a} \partial_\mu \bar{K} \boldsymbol{\tau} \cdot \mathbf{a}^{\mu\nu} \partial_\nu K. \quad (\text{A16})$$

Using $\Gamma(a_2 \rightarrow K\bar{K}) \approx 5.24$ MeV, we obtain

$$G_{aKK} = 4.89 = 0.85G_{f\pi\pi}. \quad (\text{A17})$$

The obtained results should be compared with the SU(3) symmetry relations, $G_{f'\pi\pi} = 0.10 G_{f\pi\pi}$, $G_{fKK} = 1.11 G_{f\pi\pi}$, $G_{f'KK} = -1.60 G_{f\pi\pi}$, and $G_{aKK} = 1.04 G_{f\pi\pi}$. The deviation from the SU(3) symmetry relations implies the SU(3) symmetry breaking effects and possibly the non-negligible glueball components in tensor mesons. Here, in the study of $K\bar{K}$ photoproduction, we use the coupling constants determined from the measured decay widths of tensor mesons.

2. Tensor meson radiative decays

First, we consider the $2^+0^-1^-$ interaction such as $a_2 \rightarrow \rho\pi$ or $a_2 \rightarrow \gamma\pi$ decays. The interaction Lagrangian reads [64]

$$\mathcal{L}_{a_2\gamma\pi} = \frac{g_{a_2\gamma\pi}}{M_a^2} \varepsilon^{\mu\nu\alpha\beta} \partial_\mu A_\nu a_{\alpha\rho}^\pm (\partial^\rho \partial_\beta \pi^\mp). \quad (\text{A18})$$

The coupling constant $g_{a_2\gamma\pi}$ is determined from the decay width of $a_2^\pm \rightarrow \pi^\pm \gamma$ as

$$g_{a_2\gamma\pi} \approx 0.96. \quad (\text{A19})$$

For the decays of a tensor meson into two photons, the most general form reads [66]

$$\langle \gamma(k)\gamma(k')|T \rangle = \frac{1}{M_T} \epsilon^\kappa \epsilon'^\lambda \epsilon^{\mu\nu} A_{\kappa\lambda\mu\nu}(k, k'), \quad (\text{A20})$$

where the form of $A_{\kappa\lambda\mu\nu}(k, k')$ is given by Eq. (30). With the above interaction, we have

$$\Gamma(T \rightarrow \gamma\gamma) = \frac{M_f}{20\pi} \left(\frac{1}{24} f_{T\gamma\gamma}^2 + g_{T\gamma\gamma}^2 \right). \quad (\text{A21})$$

Since

$$\begin{aligned}
\Gamma(f_2 \rightarrow \gamma\gamma)_{\text{expt.}} &= 2.6 \pm 0.24 \text{ keV}, \\
\Gamma(a_2 \rightarrow \gamma\gamma)_{\text{expt.}} &= 1.0 \pm 0.06 \text{ keV}, \\
\Gamma(f'_2 \rightarrow \gamma\gamma)_{\text{expt.}} &= 9.35 \times 10^{-2} \text{ keV},
\end{aligned}
\tag{A22}$$

we get

$$g_{f\gamma\gamma} = 0.011, \quad g_{a\gamma\gamma} = 6.9 \times 10^{-3}, \quad g_{f'\gamma\gamma} = -1.96 \times 10^{-3}, \tag{A23}$$

assuming $f_{T\gamma\gamma} = 0$.

The above interaction form can be used for the interactions of a tensor meson with a vector meson and a photon, which gives

$$\Gamma(T \rightarrow V\gamma) = \frac{M_T}{10\pi} g_{TV\gamma}^2 (1-x)^3 \left(1 + \frac{x}{2} + \frac{x^2}{6}\right), \tag{A24}$$

with $x = M_V^2/M_T^2$. There is no experimental data for this decay, so we use the predictions of Ref. [68] based on a covariant quark model, which gives a reasonable description of the known radiative decay widths of vector and tensor mesons. The predictions and the obtained coupling constants are given in Table II.

APPENDIX B: FORM FACTORS AND GAUGE INVARIANCE

Here, we discuss how we restore gauge invariance with the form factors in the form of Eq. (28). Since introducing form factors breaks gauge invariance, we use the methods of Refs. [32, 33, 34], namely, gauge invariance is satisfied by introducing contact diagrams, which effectively changes the form factors into a universal form factor. For example, let us assume we have two diagrams, a and b , which satisfy gauge invariance without form factors. The corresponding form factors F_a and F_b as functions of Mandelstam variables break the gauge invariance. Introducing contact diagrams effectively gives the universal form factor which is a constant [32] or in the form of [33],

$$F_a, F_b \rightarrow \frac{1}{2}(F_a + F_b). \tag{B1}$$

It was pointed out by Ref. [34] that such a choice would not satisfy crossing symmetry and another form was suggested, although not unique,

$$F_a, F_b \rightarrow 1 - (1 - F_a)(1 - F_b). \tag{B2}$$

In this work, we employ and extend the method of Ref. [34] for the diagrams which spoil gauge invariance due to form factors. But we do not make any modification to the purely transverse amplitudes, such as the terms with K^* exchanges and photo-transitions among hadrons, which are constructed to be gauge-invariant by themselves individually. For later use, we define the Mandelstam variables as

$$\begin{aligned}
s &= (k + p_1)^2, & s_1 &= (q_1 + q_2)^2, & s_2 &= (q_1 + p_2)^2, & s_3 &= (q_2 + p_2)^2, \\
t_1 &= (k - q_1)^2, & t_2 &= (k - q_2)^2, & t_3 &= (k - p_2)^2, \\
t_4 &= (p_1 - q_1)^2, & t_5 &= (p_1 - q_2)^2, & t_6 &= (p_1 - p_2)^2,
\end{aligned}
\tag{B3}$$

where the momenta of the initial photon and the nucleon are k and p_1 , respectively, while those of \bar{K} , K , and the final nucleon are q_1 , q_2 , and p_2 , respectively.

1. Drell diagrams

Among the possible Drell diagrams depicted in Fig. 1, those diagrams with intermediate K^* have transverse amplitude only, i.e., each diagram satisfied gauge invariance individually and introducing form factors does not spoil the gauge invariance. The gauge invariance problem occurs only when we have intermediate K and \bar{K} mesons, namely, $\gamma p \rightarrow K^+ K^- p$ and $\gamma n \rightarrow K^+ K^- n$, since they do not contribute to the reactions of $\gamma p \rightarrow K^0 \bar{K}^0 p$ and $\gamma n \rightarrow K^0 \bar{K}^0 n$. Then the amplitude takes a form of

$$\mathcal{M}^\mu = \mathcal{M}_a^\mu F_a + \mathcal{M}_b^\mu F_b + \mathcal{M}_c^\mu F_c, \quad (\text{B4})$$

where

$$F_a = \mathcal{F}(t_2, M_K^2) \mathcal{F}(t_6, M_V^2), \quad F_b = \mathcal{F}(t_1, M_K^2) \mathcal{F}(t_6, M_V^2), \quad F_c = \mathcal{F}(t_6, M_V^2), \quad (\text{B5})$$

where

$$\mathcal{F}(t_2, M_K^2) = F(t_2, M_K^2)^2, \quad \mathcal{F}(t_1, M_K^2) = F(t_1, M_K^2)^2, \quad \mathcal{F}(t_6, M_V^2) = F(t_6, M_V^2)^2, \quad (\text{B6})$$

and the form of $F(r, M^2)$ is defined in Eq. (28). One can verify that the amplitude (B4) satisfies gauge invariance when the form factors are set to be 1,

$$k \cdot \mathcal{M} = k \cdot (\mathcal{M}_a + \mathcal{M}_b + \mathcal{M}_c) = 0. \quad (\text{B7})$$

The condition, $k \cdot \mathcal{M}$, is satisfied by introducing the contact diagrams, which effectively replaces F_a , F_b , and F_c by

$$1 - (1 - F_a)(1 - F_b)(1 - F_c). \quad (\text{B8})$$

2. Vector meson and Tensor meson parts

Since the form factors and their cutoff parameters are fixed by vector meson photoproduction and tensor meson photoproduction processes where the vector or tensor mesons are on mass-shell, we need to include the form factors in order to take into account the off-shell-ness of the intermediate vector/tensor mesons. Furthermore, the amplitudes $\mathcal{M}^{\mu\nu}$ of Eq. (17) and $\mathcal{M}^{\mu, \alpha\beta}$ of Eq. (19) are constructed to satisfy the gauge invariance condition. So the form factor which should be multiplied in addition to the form factors for vector/tensor meson photoproduction part reads

$$F = F(s_1, M^2)^2, \quad (\text{B9})$$

where M is the vector meson or tensor meson mass.

3. Intermediate hyperons

a. Intermediate spin-1/2 hyperons

In this case, since we adopt the pseudoscalar coupling, we have five diagrams as shown in Figs. 5(a)-(e). The possible intermediate states are $\Lambda(1116)$, $\Lambda(1405)$, and $\Sigma(1193)$. We

first consider the case of $\Sigma(1193)$, which have the properties as

$$\begin{aligned}
k \cdot \mathcal{M}_c^n &= 0, & k \cdot \mathcal{M}_d^{\Sigma^0} &= 0, & k \cdot \mathcal{M}_e^n &= 0, \\
k \cdot \mathcal{M}_d^{\Sigma^+} &= k \cdot \mathcal{M}_b + k \cdot \mathcal{M}_a = -k \cdot \mathcal{M}_e^p - k \cdot \mathcal{M}_c^p, \\
k \cdot \mathcal{M}_a + k \cdot \mathcal{M}_c^p &= 0, & k \cdot \mathcal{M}_b + k \cdot \mathcal{M}_e^p &= 0,
\end{aligned} \tag{B10}$$

where the superscripts p, n denote the proton and neutron, respectively, and the subscripts specify the diagram in Fig. 5.

For $\gamma p \rightarrow K^+ K^- p$, we have

$$\mathcal{M}^\mu = \mathcal{M}_a^\mu F_a + \mathcal{M}_b^\mu F_b + \mathcal{M}_c^{p,\mu} F_c + \mathcal{M}_d^{\Sigma^0,\mu} F_d + \mathcal{M}_e^{p,\mu} F_e. \tag{B11}$$

Because of the properties of Eq. (B10), we have $k \cdot \mathcal{M} = 0$ without form factors. Since the amplitudes \mathcal{M}_a and \mathcal{M}_c correspond to a part of Λ photoproduction, which should have nontrivial form factors, we replace the form factors as

$$F_a, F_c \rightarrow \{1 - (1 - F(t_2, M_K^2)^2)(1 - F(s, M_N^2)^2)\} F(s_2, M_\Sigma^2)^2. \tag{B12}$$

Similarly,

$$F_b, F_e \rightarrow \{1 - (1 - F(t_1, M_K^2)^2)(1 - F(t_3, M_N^2)^2)\} F(t_5, M_\Sigma^2)^2, \tag{B13}$$

so that gauge invariance is now satisfied with the form factors.

For $\gamma p \rightarrow K^0 \bar{K}^0 p$, we have

$$\mathcal{M}^\mu = 2(\mathcal{M}_c^{p,\mu} F_c + \mathcal{M}_d^{\Sigma^+,\mu} F_d + \mathcal{M}_e^{p,\mu} F_e), \tag{B14}$$

where the form factors F_c , F_d , and F_e are replaced by

$$1 - (1 - F_c)(1 - F_d)(1 - F_e). \tag{B15}$$

For $\gamma n \rightarrow K^+ K^- n$, we have

$$\mathcal{M}^\mu = 2(\mathcal{M}_a^\mu F_a + \mathcal{M}_b^\mu F_b + \mathcal{M}_c^{n,\mu} F_c + \mathcal{M}_d^{\Sigma^-, \mu} F_d + \mathcal{M}_e^{n,\mu} F_e), \tag{B16}$$

where the form factors F_a , F_b , and F_d are replaced by

$$1 - (1 - F_a)(1 - F_b)(1 - F_d). \tag{B17}$$

Since $\mathcal{M}_c^{n,\mu}$ and $\mathcal{M}_e^{n,\mu}$ are transverse, the form factors F_c and F_e are not changed.

For $\gamma n \rightarrow K^0 \bar{K}^0 n$, we have

$$\mathcal{M}^\mu = \mathcal{M}_c^{n,\mu} F_c + \mathcal{M}_d^{\Sigma^0,\mu} F_d + \mathcal{M}_e^{n,\mu} F_e. \tag{B18}$$

Since all the amplitudes are transverse, they are gauge invariant.

The intermediate $\Lambda(1116)$ and $\Lambda(1405)$ states are the same as the case of Σ^0 . As a consequence, these intermediate states do not exist for the $\gamma p \rightarrow K^0 \bar{K}^0 p$ and $\gamma n \rightarrow K^+ K^- n$ reactions. We replace the form factors as in Eq. (B11) for $\gamma p \rightarrow K^+ K^- p$. The amplitudes for $\gamma n \rightarrow K^0 \bar{K}^0 n$ are all transverse.

b. Intermediate spin-3/2 hyperons

The intermediate states $\Sigma(1385)$ and $\Lambda(1520)$ contain seven diagrams shown in Figs. 5(a)-(g), which satisfy

$$\begin{aligned}
k \cdot \mathcal{M}_c^n &= 0, & k \cdot \mathcal{M}_d^{\Sigma^{*0}} &= 0, & k \cdot \mathcal{M}_e^n &= 0, \\
k \cdot \mathcal{M}_d^{\Sigma^{*+}} &= -k \cdot \mathcal{M}_d^{\Sigma^{*-}} = -k \cdot \mathcal{M}_c^p - k \cdot \mathcal{M}_e^p, \\
k \cdot \mathcal{M}_a + k \cdot \mathcal{M}_c^p + k \cdot \mathcal{M}_f &= 0, \\
k \cdot \mathcal{M}_b + k \cdot \mathcal{M}_e^p + k \cdot \mathcal{M}_g &= 0,
\end{aligned} \tag{B19}$$

for the case of intermediate $\Sigma^*(1385)$.

For $\gamma p \rightarrow K^+ K^- p$, we have

$$\mathcal{M}^\mu = \mathcal{M}_a^\mu F_a + \mathcal{M}_b^\mu F_b + \mathcal{M}_c^{p,\mu} F_c + \mathcal{M}_d^{\Sigma^{*0},\mu} F_d + \mathcal{M}_e^{p,\mu} F_e + \mathcal{M}_f^\mu F_f + \mathcal{M}_g^\mu F_g. \tag{B20}$$

In this case, the direct application of the method of Ref. [34],

$$F_a, F_c, F_f \rightarrow 1 - (1 - F_a)(1 - F_c)(1 - F_f), \quad F_b, F_e, F_g \rightarrow 1 - (1 - F_b)(1 - F_e)(1 - F_g), \tag{B21}$$

cannot be used. This is because the above form factor becomes 1 if, for example, any of (F_a, F_c, F_f) is 1. And this in fact happens when the intermediate Σ^* becomes on mass-shell, $s_2 = M_{\Sigma^*}^2$ since $F_f = F(s_2, M_{\Sigma^*}^2)^2$. Since these diagrams are a part of photoproduction of K and Σ^* , this means that those amplitudes have no form factor. Therefore, instead of Eq. (B21), we replace the form factors as

$$\begin{aligned}
F_a, F_c, F_f &\rightarrow \{1 - (1 - F(t_2, M_K^2)^2)(1 - F(s, M_N^2)^2)\} F(s_2, M_{\Sigma^*}^2)^2, \\
F_b, F_e, F_g &\rightarrow \{1 - (1 - F(t_1, M_K^2)^2)(1 - F(t_3, M_N^2)^2)\} F(t_5, M_{\Sigma^*}^2)^2.
\end{aligned} \tag{B22}$$

For $\gamma p \rightarrow K^0 \bar{K}^0 p$, we have

$$\mathcal{M}^\mu = 2(\mathcal{M}_c^{p,\mu} F_c + \mathcal{M}_d^{\Sigma^{*+},\mu} F_d + \mathcal{M}_e^{p,\mu} F_e). \tag{B23}$$

The form factors F_c , F_d , and F_e are replaced by

$$1 - (1 - F_c)(1 - F_d)(1 - F_e). \tag{B24}$$

For $\gamma n \rightarrow K^+ K^- n$, we have

$$\mathcal{M}^\mu = 2(\mathcal{M}_a^\mu F_a + \mathcal{M}_b^\mu F_b + \mathcal{M}_c^{n,\mu} F_c + \mathcal{M}_d^{\Sigma^{*-},\mu} F_d + \mathcal{M}_e^{n,\mu} F_e + \mathcal{M}_f^\mu F_f + \mathcal{M}_g^\mu F_g), \tag{B25}$$

where the form factors F_a , F_b , F_d , F_f , and F_g are

$$1 - (1 - F_a)(1 - F_b)(1 - F_d)(1 - F_f)(1 - F_g), \tag{B26}$$

and

$$F_f' = F_g' = F_f F_g, \tag{B27}$$

which is chosen to avoid the problem mentioned above.

For $\gamma n \rightarrow K^0 \bar{K}^0 n$, we have

$$\mathcal{M}^\mu = \mathcal{M}_c^{n,\mu} F_c + \mathcal{M}_d^{\Sigma^{*0},\mu} F_d + \mathcal{M}_e^{n,\mu} F_e. \tag{B28}$$

In this case, all amplitudes are gauge-invariant, we do not introduce any contact diagrams.

The case of intermediate $\Lambda(1520)$ is the same as in the case of $\Sigma^0(1385)$. So it does not contribute to the $\gamma p \rightarrow K^0 \bar{K}^0 p$ and $\gamma n \rightarrow K^+ K^- n$ reactions.

4. Intermediate Θ

This case is similar to the case of intermediate Λ except that Θ has positive charge. The K^* exchange diagrams, Figs. 6(f,g), are transverse, so gauge invariance is satisfied even with the presence of form factors. The amplitudes of Fig. 6 satisfy

$$\begin{aligned} k \cdot \mathcal{M}_c^n &= 0, & k \cdot \mathcal{M}_e^n &= 0, \\ k \cdot \mathcal{M}_a + k \cdot \mathcal{M}_b + k \cdot \mathcal{M}_d &= 0, \\ k \cdot \mathcal{M}_c + k \cdot \mathcal{M}_d + k \cdot \mathcal{M}_e &= 0. \end{aligned} \tag{B29}$$

For $\gamma p \rightarrow K^0 \bar{K}^0 p$, we have

$$\mathcal{M}^\mu = \mathcal{M}_c^{p,\mu} F_c + \mathcal{M}_d^\mu F_d + \mathcal{M}_e^{p,\mu} F_e + \mathcal{M}_f^\mu F_f + \mathcal{M}_g^\mu F_g, \tag{B30}$$

where

$$F_c, F_d, F_e \rightarrow 1 - (1 - F_c)(1 - F_d)(1 - F_e). \tag{B31}$$

For $\gamma n \rightarrow K^+ K^- n$, we have

$$\mathcal{M}^\mu = \mathcal{M}_a F_a + \mathcal{M}_b F_b \mathcal{M}_c^{n,\mu} F_c + \mathcal{M}_d^\mu F_d + \mathcal{M}_e^{n,\mu} F_e + \mathcal{M}_f^\mu F_f + \mathcal{M}_g^\mu F_g, \tag{B32}$$

where

$$F_a, F_b, F_d \rightarrow 1 - (1 - F_a)(1 - F_b)(1 - F_d). \tag{B33}$$

-
- [1] LEPS Collaboration, T. Nakano *et al.*, Phys. Rev. Lett. **91**, 012002 (2003).
 - [2] DIANA Collaboration, V.V. Barmin *et al.*, Yad. Fiz. **66**, 1763 (2003), [Phys. At. Nucl. **66**, 1715 (2003)].
 - [3] CLAS Collaboration, S. Stepanyan *et al.*, Phys. Rev. Lett. **91**, 252001 (2003).
 - [4] SAPHIR Collaboration, J. Barth *et al.*, Phys. Lett. B **572**, 127 (2003).
 - [5] A.E. Asratyan, A.G. Dolgolenko, and M.A. Kubantsev, Yad. Fiz. **67**, 704 (2004), [Phys. Atom. Nucl. **67**, 682 (2004)].
 - [6] CLAS Collaboration, V. Kubarovsky *et al.*, Phys. Rev. Lett. **92**, 032001 (2004).
 - [7] HERMES Collaboration, A. Airapetian *et al.*, Phys. Lett. B **585**, 213 (2004).
 - [8] P.Zh. Aslanyan, V.N. Emelyanenko, and G.G. Rikhkvitckaya, hep-ex/0403044.
 - [9] COSY-TOF Collaboration, M. Abdel-Bary *et al.*, Phys. Lett. B **595**, 127 (2004).
 - [10] ZEUS Collaboration, S. Chekanov *et al.*, Phys. Lett. B **591**, 7 (2004).
 - [11] SVD Collaboration, A. Aleev *et al.*, hep-ex/0401024.
 - [12] NA49 Collaboration, C. Alt *et al.*, Phys. Rev. Lett. **92**, 042003 (2004).
 - [13] H1 Collaboration, A. Aktas *et al.*, Phys. Lett. B **588**, 17 (2004).
 - [14] SPHINX Collaboration, Yu.M. Antipov *et al.*, hep-ex/0407026.
 - [15] C. Pinkenburg, J. Phys. G **30**, S1201 (2004).
 - [16] D.O. Litvintsev for the CDF Collaboration, hep-ex/0410024.
 - [17] HyperCP Collaboration, M.J. Longo *et al.*, hep-ex/0410027.
 - [18] T. Berger-Hryn'ova for the BABAR Collaboration, hep-ex/0411017.
 - [19] HERA-B Collaboration, I. Abt *et al.*, hep-ex/0408048.

- [20] BES Collaboration, M. Ablikim *et al.*, Phys. Rev. D **70**, 012004 (2004).
- [21] L.G. Landsberg, Phys. Rep. **320**, 223 (1999).
- [22] BES Collaboration, M. Ablikim *et al.*, hep-ex/0405030.
- [23] V. Kuznetsov, hep-ex/0409032.
- [24] P.A. Żołnierczuk, D.S. Armstrong, E. Christy, J.H.D. Clark, T.P. Gorringer, M.D. Hasinoff, M.A. Kovash, S.Tripathi, and D.H. Wright, Phys. Lett. B **597**, 131 (2004); B. Tatischeff, nucl-ex/0404042.
- [25] H.G. Juengst for the CLAS Collaboration, hep-ex/0312019; K. Hicks, hep-ph/0408001; V.D. Burkert, R. de Vita, and S. Niccolai for the CLAS Collaboration, nucl-ex/0408019; V. Kubarovsky and P. Stoler for the CLAS Collaboration, hep-ex/0409025; Y. Ohashi for the LEPS Collaboration, hep-ex/0402005.
- [26] A.R. Dzierba, D. Krop, M. Swat, S. Teige, and A.P. Szczepaniak, Phys. Rev. D **69**, 051901 (2004).
- [27] J. Tyson, J.S. Greenberg, V.W. Hughes, D.C. Lu, R.C. Minehart, S. Mori, and J.E. Rothberg, Phys. Rev. Lett. **19**, 255 (1967).
- [28] K. Nakayama and K. Tsushima, Phys. Lett. B **583**, 269 (2004).
- [29] E.W. Anderson *et al.*, Phys. Lett. **29B**, 136 (1969).
- [30] W. Roberts, nucl-th/0408034; nucl-th/0412041.
- [31] A.I. Titov, H. Ejiri, H. Haberzettl, and K. Nakayama, nucl-th/0410098.
- [32] K. Ohta, Phys. Rev. C **40**, 1335 (1989).
- [33] H. Haberzettl, Phys. Rev. C **56**, 2041 (1997); H. Haberzettl, C. Bennhold, T. Mart, and T. Feuster, Phys. Rev. C **58**, 40 (1998).
- [34] R.M. Davidson and R. Workman, Phys. Rev. C **63**, 025210 (2001).
- [35] Y. Oh and H. Kim, Phys. Rev. D **70**, 094022 (2004); Y. Oh, H. Kim, and S.H. Lee, Phys. Rev. D **69**, 094009 (2004).
- [36] C.E. Carlson, C.D. Carone, H.J. Kwee, and V. Nazaryan, Phys. Lett. B **573**, 101 (2003).
- [37] S.-L. Zhu, Phys. Rev. Lett. **91**, 232002 (2003); J. Sugiyama, T. Doi, and M. Oka, Phys. Lett. B **581**, 167 (2004).
- [38] F. Csikor, Z. Fodor, S.D. Katz, and T.G. Kovács, JHEP **0311**, 070 (2003); S. Sasaki, Phys. Rev. Lett. **93**, 152001 (2004); N. Mathur *et al.*, hep-ph/0406196.
- [39] C.E. Carlson, C.D. Carone, H.J. Kwee, and V. Nazaryan, Phys. Lett. B **579**, 52 (2004).
- [40] R. Jaffe and F. Wilczek, Phys. Rev. Lett. **91**, 232003 (2003).
- [41] M. Karliner and H.J. Lipkin, hep-ph/0307243.
- [42] D. Diakonov, V. Petrov, and M. Polyakov, Z. Phys. A **359**, 305 (1997).
- [43] T.-W. Chiu and T.-H. Hsieh, hep-ph/0403020.
- [44] H. Kim, S.H. Lee, and Y. Oh, Phys. Lett. B **595**, 293 (2004).
- [45] M. Oka, hep-ph/0409295; S.H. Lee, H. Kim, and Y. Kwon, hep-ph/0411104; R.D. Matheus and S. Narison, hep-ph/0412063; H.-J. Lee, N.I. Kochelev, and V. Vento, hep-ph/0412127.
- [46] Y. Oh, H. Kim, and S.H. Lee, Nucl. Phys. **A745**, 129 (2004).
- [47] W. Liu and C.M. Ko, Nucl. Phys. **A741**, 215 (2004); nucl-th/0410068; W. Liu, C.M. Ko, and V. Kubarovsky, Phys. Rev. C **69**, 025202 (2004).
- [48] S.I. Nam, A. Hosaka, and H.-C. Kim, hep-ph/0403009.
- [49] Y. Oh, H. Kim, and S.H. Lee, Phys. Rev. D **69**, 014009 (2004); Phys. Rev. D **69**, 074016 (2004).
- [50] Q. Zhao and J.S. Al-Khalili, Phys. Lett. B **585**, 91 (2004), **596**, 317(E) (2004).
- [51] K. Nakayama and W.G. Love, Phys. Rev. C **70**, 012201 (2004).

- [52] A.W. Thomas, K. Hicks, and A. Hosaka, *Prog. Theor. Phys.* **111**, 291 (2004).
- [53] C. Hanhart, M. Büscher, W. Eyrich, K. Kilian, U.-G. Meißner, F. Rathmann, A. Sibirtsev, and H. Ströher, *Phys. Lett. B* **590**, 39 (2004); C. Hanhart, J. Haidenbauer, K. Nakayama, and U.-G. Meißner, hep-ph/0407107; Yu.N. Uzikov, nucl-th/0411113.
- [54] T. Hyodo, A. Hosaka, and E. Oset, *Phys. Lett. B* **579**, 290 (2004).
- [55] B.-G. Yu, T.-K. Choi, and C.-R. Ji, *Phys. Rev. C* **70**, 045205 (2004).
- [56] T. Sato and T.-S.H. Lee, *Phys. Rev. C* **54**, 2660 (1996).
- [57] R. Machleidt, K. Holinde, and C. Elster, *Phys. Rep.* **149**, 1 (1987).
- [58] M. Bando, T. Kugo, and K. Yamawaki, *Phys. Rep.* **164**, 217 (1988).
- [59] Particle Data Group, S. Eidelman *et al.*, *Phys. Lett. B* **592**, 1 (2004).
- [60] Y. Oh, A.I. Titov, and T.-S.H. Lee, in *NSTAR2000 Workshop: Excited Nucleons and Hadronic Structure*, edited by V. D. Burkert, L. Elouadrhiri, J. J. Kelly, and R. C. Minehart, (World Scientific, Singapore, 2000), pp. 255–262, nucl-th/0004055; Y. Oh, A.I. Titov, and T.-S.H. Lee, *Phys. Rev. C* **63**, 025201 (2001); Y. Oh and T.-S.H. Lee, *Phys. Rev. C* **66**, 045201 (2002); *Phys. Rev. C* **69**, 025201 (2004).
- [61] Y. Eisenberg *et al.*, *Phys. Rev. Lett.* **23**, 1322 (1969).
- [62] Y. Eisenberg *et al.*, *Phys. Rev. D* **5**, 15 (1972).
- [63] G.T. Condo, T. Handler, W.M. Bugg, G.R. Blakett, M. Pisharody, and K.A. Danyo, *Phys. Rev. D* **48**, 3045 (1993); A.V. Afanasev and A.P. Szczepaniak, *Phys. Rev. D* **61**, 114008 (2000).
- [64] H. Högaasen, J. Högaasen, R. Keyser, and B.E.Y. Svensson, *Nouvo Cimento* **42A**, 323 (1966).
- [65] E.R. Berger, A. Donnachie, H.G. Dosch, and O. Nachtmann, *Eur. Phys. J. C* **14**, 673 (2000).
- [66] B. Renner, *Nucl. Phys.* **B30**, 634 (1971).
- [67] P. Singer, *Phys. Rev. D* **27**, 2223 (1983).
- [68] S. Ishida, K. Yamada, and M. Oda, *Phys. Rev. D* **40**, 1497 (1989).
- [69] Aachen-Hamburg-Heidelberg-München Collaboration, W. Struczinski *et al.*, *Nucl. Phys.* **B108**, 45 (1976).
- [70] M. El Amiri, G. López Castro, and J. Pestieau, *Nucl. Phys.* **A543**, 673 (1992).
- [71] D. Lin, M.K. Liou, and Z.M. Ding, *Phys. Rev. C* **44**, 1819 (1991).
- [72] R.M. Davidson, N.C. Mukhopadhyay, and R.S. Wittman, *Phys. Rev. D* **43**, 71 (1991).
- [73] M. Benmerrouche, R.M. Davidson, and N.C. Mukhopadhyay, *Phys. Rev. C* **39**, 2339 (1989).
- [74] M. Benmerrouche, N.C. Mukhopadhyay, and J.F. Zhang, *Phys. Rev. D* **51**, 3237 (1995).
- [75] Th.A. Rijken, V.G.J. Stoks, and Y. Yamamoto, *Phys. Rev. C* **59**, 21 (1999); V.G.J. Stoks and Th.A. Rijken, *Phys. Rev. C* **59**, 3009 (1999).
- [76] S. Deser, A. Waldron, and V. Pascalutsa, *Phys. Rev. D* **62**, 105031 (2000).
- [77] D.B. Lichtenberg, *Phys. Rev. D* **15**, 345 (1977).
- [78] J.W. Darewych, M. Horbatsch, and R. Koniuk, *Phys. Rev. D* **28**, 1125 (1983).
- [79] G.E. Brown and W. Weise, *Phys. Rep.* **22**, 279 (1975).
- [80] H. Kammano and M. Arima, *Phys. Rev. C* **69**, 025206 (2004).
- [81] C.L. Schat, N.N. Scoccola, and C. Gobbi, *Nucl. Phys.* **A585**, 627 (1995).
- [82] D. Jido, A. Hosaka, J.C. Nacher, E. Oset, and A. Ramos, *Phys. Rev. C* **66**, 025203 (2002).
- [83] SPHINX Collaboration, Yu.M. Antipov *et al.*, *Phys. Lett. B* **604**, 22 (2004).
- [84] R.A. Arndt, I.I. Strakovsky, and R.L. Workman, *Phys. Rev. C* **68**, 042201 (2003), **69**, 019901(E) (2004).
- [85] F.E. Close and J.J. Dudek, *Phys. Lett. B* **586**, 75 (2004).
- [86] C.E. Carlson, C.D. Carone, H.J. Kwee, and V. Nazaryan, *Phys. Rev. D* **70**, 037501 (2004).

- [87] R. Bijker, M.M. Giannini, and E. Santopinto, Phys. Lett. B **595**, 260 (2004).
- [88] ABBHHM Collaboration, R. Erbe *et al.*, Phys. Rev. **188**, 2060 (1969).
- [89] J. Ballam *et al.*, Phys. Rev. D **5**, 545 (1972).
- [90] K. Hicks, V. Burkert, A.E. Kudryavtsev, I.I. Strakovsky, and S. Stepanyan, hep-ph/0411265.